

# **Photoproduction of $\pi^0$ on hydrogen with CLAS from 1.1 GeV - 5.45 GeV from $e^+e^-\gamma$ decay**

**Michael C. Kunkel**

**Old Dominion University**

1 Introduction

2  $\pi^0$  production

3  $\pi^0$  decay

4 CLAS Setup and G12  
Experiment

5 Simulation

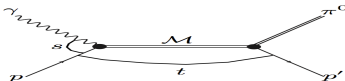
6 Results

- Systematics
- Normalization
- Cross-Sections
  - Differential Cross-Section  
 $\cos \theta$  vs.  $\frac{d\sigma}{d\Omega}$
  - Differential Cross-Section  
 $W$  vs.  $\frac{d\sigma}{d\Omega}$
  - Differential Cross-Section  
 $|t|$  vs.  $\frac{d\sigma}{dt}$

7 Conclusions

- We performed precise measurements of the  $\pi^0$  cross-section
  - Compare to existing data
  - Check validity of handbag model
- Improve understanding of the  $\pi^0$  production in
  - standard model applicable at lower energies
- New model applying the GPD handbag model applicable at higher energies

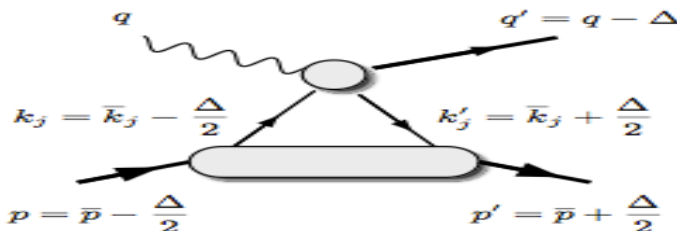
# $\pi^0$ production



- $$\frac{d\sigma}{d\Omega} = \frac{q}{k} |\langle \chi_f | \mathcal{M} | \chi_i \rangle|^2$$
- $$\frac{d\sigma}{d\Omega} = \frac{1}{2} \frac{q}{k} \left( |H_N|^2 + |H_D|^2 + |H_{SP}|^2 + |H_{SA}|^2 \right)$$
  - $H_N \equiv$  non-flip amplitudes
  - $H_D \equiv$  double-flip amplitudes
  - $H_{SP} \equiv$  single-flip amplitudes initial photon and nucleon having spins parallel
  - $H_{SA} \equiv$  single-flip amplitudes initial photon and nucleon having spins anti-parallel
- Amplitudes have different kinematic dependence
- Amplitudes are common to different reactions i.e.  
 $\gamma p \rightarrow n\pi^+, \gamma p \rightarrow p\pi^0, \gamma n \rightarrow n\pi^-$
- Model valid below 2.8 GeV currently

## $\pi^0$ Production above 2.8 GeV

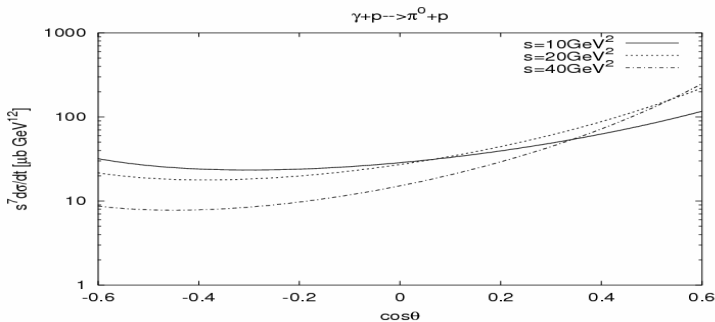
- $\pi^0$  production is factorized into two parts
  - one quark from the incoming and one from the outgoing nucleon participate in the hard sub-process (small blob)
    - calculable using PQCD
  - The soft part consists of all the other partons that are spectators and can be described in terms of GPDs (large blob)



The handbag-type diagram for photoproduction of mesons.

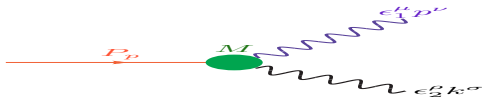
# $\pi^0$ Production above 2.8 GeV

- Recent framework of handbag model led to  $\pi^0$  cross-section predictions

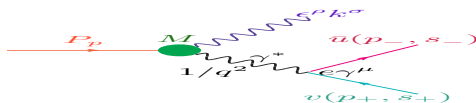


The soft physics contribution to the cross-section for photoproduction of  $\pi^0$  scaled by  $s^7$  versus  $\cos\theta$ , where  $\theta$  is the scattering angle in the  $\gamma p$  c.m. system and  $s$  is the total invariant energy squared.

# $\pi^0$ Decay Modes



(a)



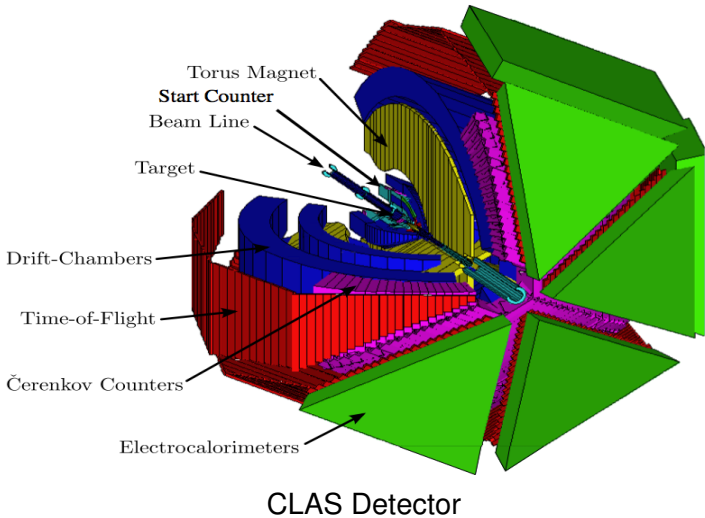
(b)

Feynman diagram of  $\pi^0$  two photon decay (a). Feynman diagram of  $\pi^0$  Dalitz decay (b).

- $\pi^0 \rightarrow \gamma\gamma$  98.8%
- $\pi^0 \rightarrow e^+e^-\gamma$  1.2%
- We choose  $e^+e^-$  for cleaner signal and trigger

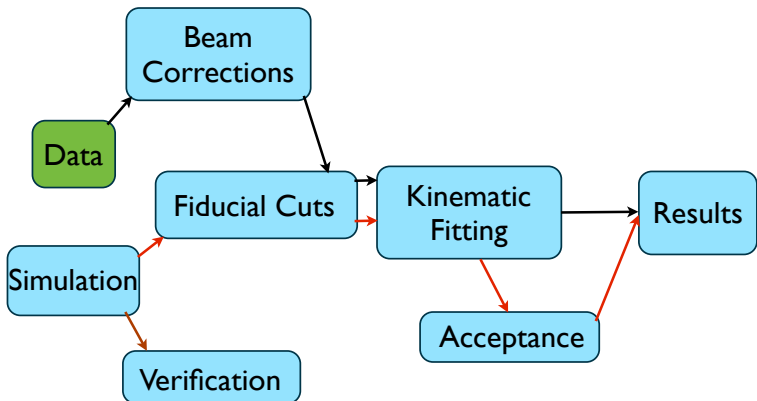
- The  $\pi^0$  decays to 2 photons 98.8%
  - Either photon has equal probability of pair producing  $e^+e^-$  pairs
  - Decay photons travel through target
    - $\langle L \rangle \approx 15$  cm
    - $\approx 1.5\%$  conversion to  $e^+e^-$
- The  $\pi^0$  decays to  $e^+e^- \gamma$  1.2%
- Total  $e^+e^- \gamma$  yield is  $\approx 2.7\%$

# CLAS Detector

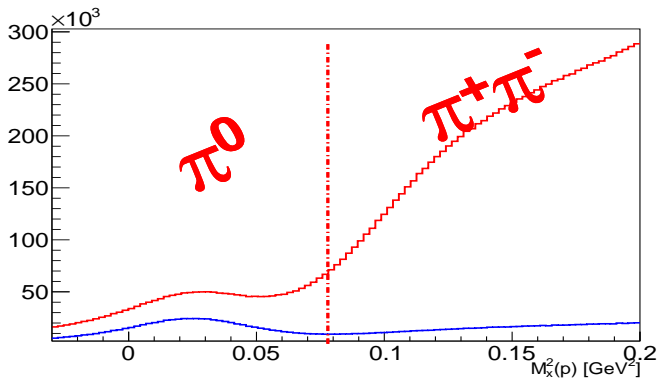


- 60-65 nA electron beam
- $E_\gamma$  up to 5.5 GeV
- $70 \cdot 10^6$  tagged photons per second
- 40 cm  $\ell\text{H}_2$  target
- 126 TB of raw data (largest to date for photo-production)
- $26.2 \times 10^9$  production triggers ( $3 \times 10^6$  di-lepton triggers)
- e/ $\pi$  rejection factor of  $10^{-6}$  for di-lepton pairs
- Trigger
  - 2 charged particles  $E_\gamma > 3.6$  GeV
  - 1 lepton plus 1 other charged particle for  $E_\gamma < 3.6$  GeV

## Procedures

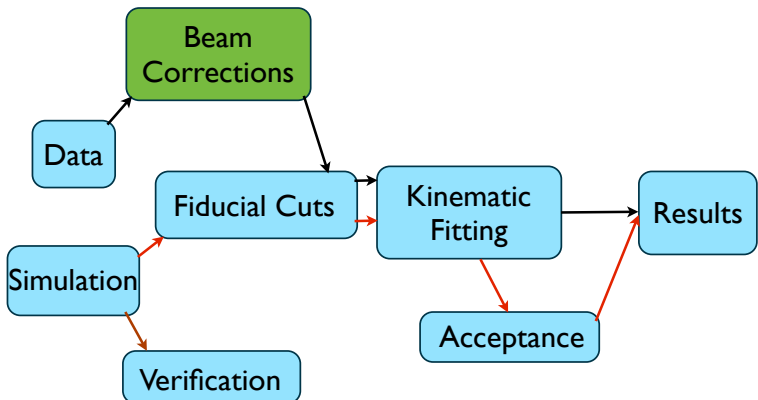


- Select  $\gamma p \rightarrow pq^+q^- (X)$  events
- Identify  $\gamma p \rightarrow pe^+e^- (X)$  events
  - Cherenkov Detector (cc) and Electromagnetic Calorimeter (EC) cuts for  $E_\gamma < 3.6$  GeV
- Kinematic fit to identify  $\gamma$  in final state
- Kinematic fit to cut out  $\gamma p \rightarrow p\pi^+\pi^-$  events
- Proton momentum corrected for energy loss in matter



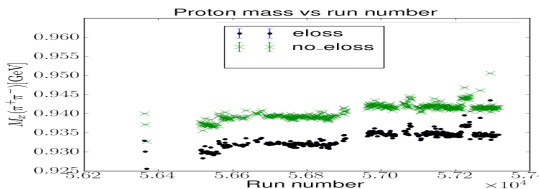
Effect of CC & EC cuts placed on data,  $E_\gamma < 3.6 \text{ GeV}$

# Beam Energy Corrections

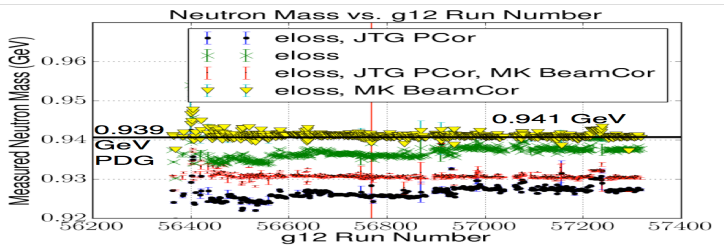


# Beam Energy Corrections

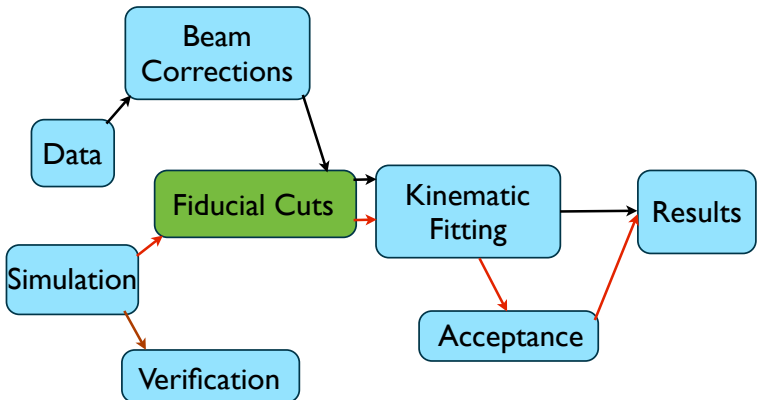
- $M_x(\gamma p \rightarrow \pi^+ \pi^- X)$  and  $M_x(\gamma p \rightarrow \pi^+ \pi^- \pi^+ X)$  were too low
- Time Dependent



- Corrected photon energies for tagger hysteresis.

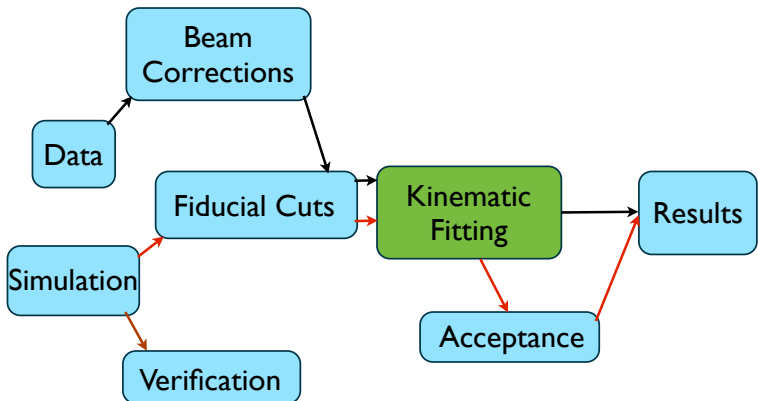


# Fiducial Cuts



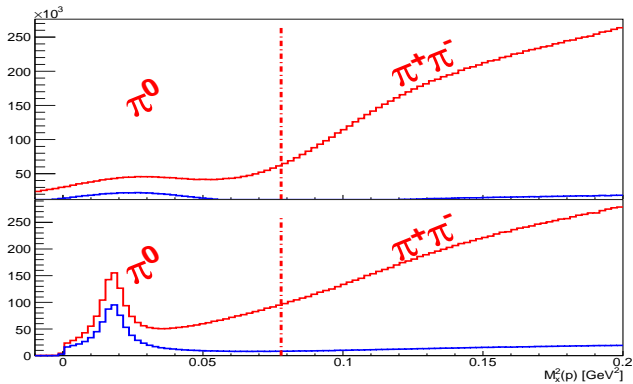
- Select regions of the detector where the acceptance is uniform
  - Geometric Fiducial Cuts
    - Events in nonuniform regions, such as space between sectors, are removed
  - EC Fiducial Cuts
    - EC sectors 1, 2, 3, **5 had dead/inefficient EC strips**
    - **Events hitting bad EC strips were removed**
  - TOF Fiducial Cuts
    - Sector 1 and 3 had dead/inefficient TOF paddles
    - Events hitting bad paddles were removed
- All cuts applied to both data and simulation

# Kinematic Fitting



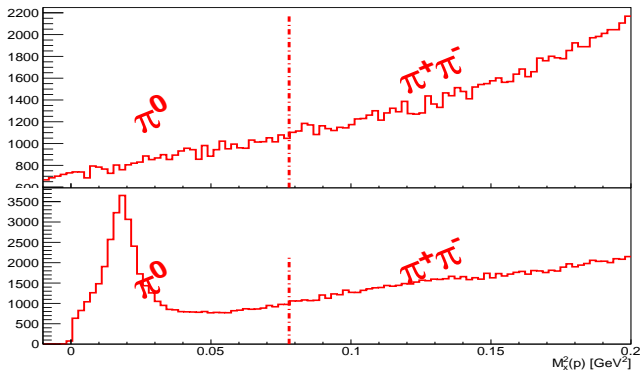
- Measured  $\gamma p \rightarrow pe^+e^-(\gamma)$  with uncertainties
- Kinematic fitter adjusts measured momenta within uncertainties by applying constraints
  - E and  $\vec{p}$  constraints
  - Particle mass constraints
- Compare hypothesis likelihoods
  - 1-C:  $pe^+e^-(\gamma)$  vs.  $pe^+e^-(X)$
  - 2-C:  $M(e^+e^-(\gamma)) = M_{\pi^0}$  vs.  $M_x$
  - 4-C:  $p\pi^+\pi^-$  single hypothesis

# Kinematic Fitting



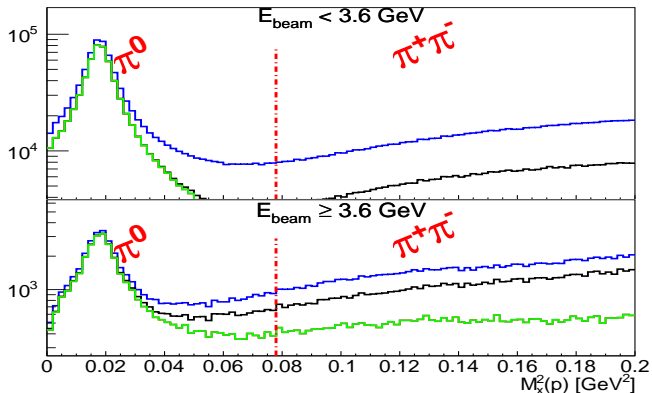
Effect of kinematic fitting, on data before 1-C kinematic fitting (top) and after (bottom),  $E_\gamma < 3.6 \text{ GeV}$ . Red solid line represents all data while the blue line depicts all data with cuts placed on CC and EC cuts. Red dashed line represents  $\pi^+\pi^-$  production threshold.

# Kinematic Fitting



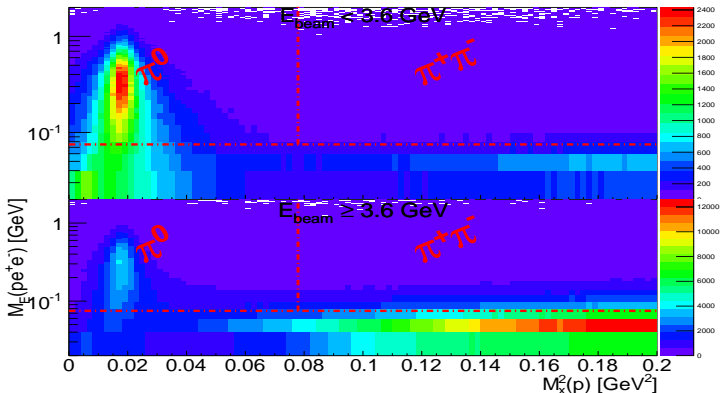
Effect of kinematic fitting, on data before 1-C kinematic fitting (top) and after (bottom),  $E_\gamma > 3.6 \text{ GeV}$ . Red dashed line represents  $\pi^+\pi^-$  production threshold.

## Kinematic Fitting Cuts



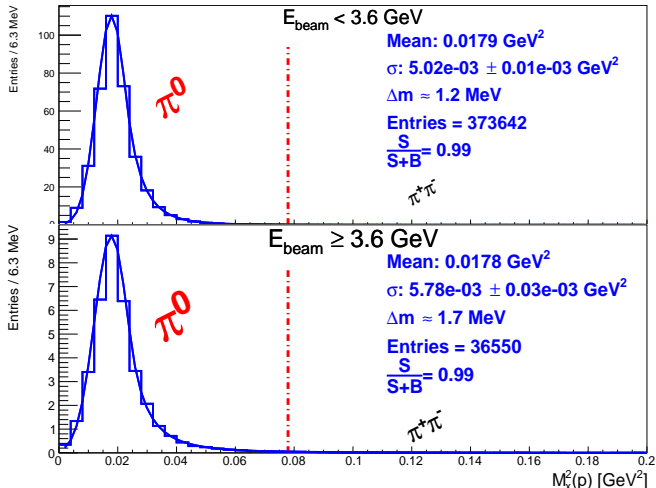
Mass squared distributions of  $M_x^2(\gamma p \rightarrow pX)$ . Blue lines depict the fitted data prior to hypothesis cuts, black line depicts after a 1% cut placed on the 1-C and green line depicts the effect of the 1% 4-C fit cut.

# Kinematic Fitting Missing Energy

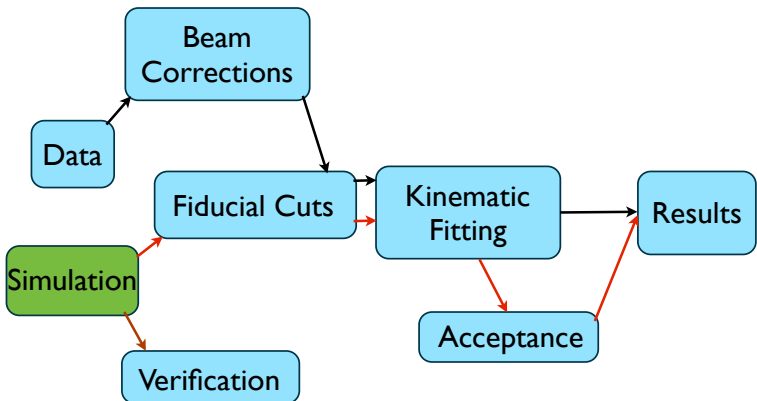


$M_E(\gamma p \rightarrow \text{pe}^+\text{e}^-)$  vs.  $M_x^2(\gamma p \rightarrow pX)$ . The horizontal red dashed-dotted line depicts the 75 MeV cut used in this analysis. The vertical red dashed-dotted line depicts boundary of single  $\pi^0$  to  $\pi^+\pi^-$  production.

# Kinematic Fitting 2C Cut

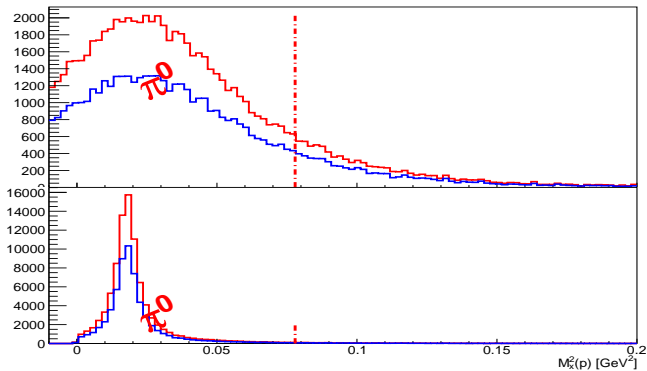


$$M_x^2(\gamma p \rightarrow pX)$$



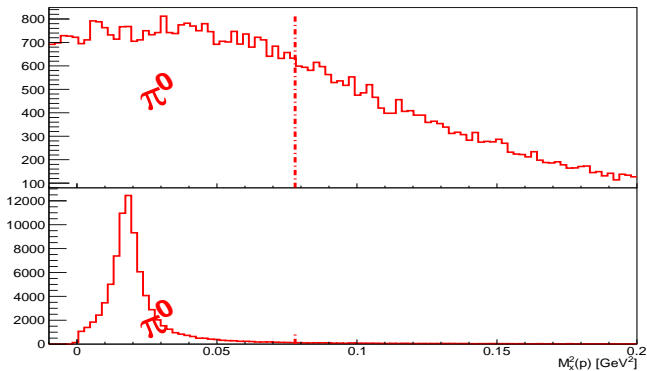
- PLUTO++ generates events
  - $\gamma p \rightarrow p\pi^0 \rightarrow pe^+e^- \gamma$
  - $\gamma p \rightarrow p\pi^+\pi^-$
  - Phasespace or Differential cross-sections
- Simulation Chain
  - PLUTO++, GSIM, GPP, A1C, Analyzer

# Kinematic Fitting Simulation



Effect of kinematic fitting, on simulation before 1-C kinematic fitting (top) and after (bottom),  $E_\gamma < 3.6 \text{ GeV}$ . Red solid line represents all data while the blue line depicts all data with cuts placed on CC and EC cuts. Red dashed line represents  $\pi^+\pi^-$  threshold.

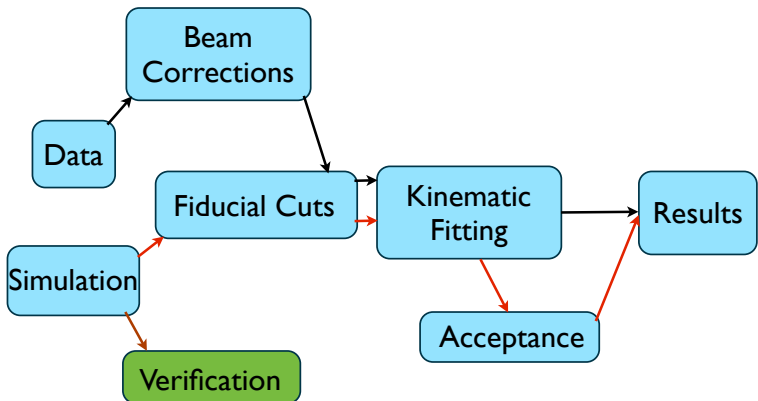
# Kinematic Fitting Simulation



Effect of kinematic fitting, on simulation before 1-C kinematic fitting (top) and after (bottom),  $E_\gamma > 3.6 \text{ GeV}$ . Red dashed line represents  $\pi^+\pi^-$  threshold.

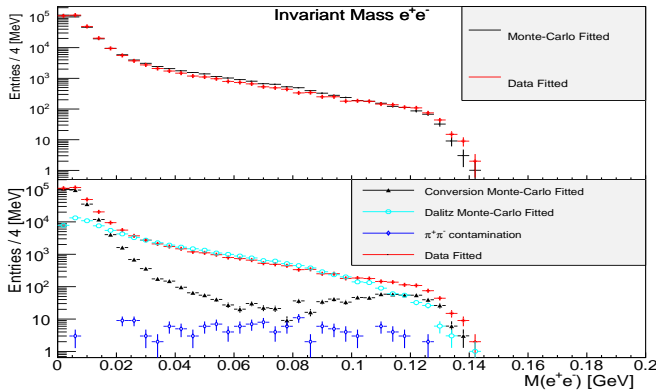
- Cuts employed
  - CC and EC hit requirements  $E_\gamma < 3.6 \text{ GeV}$
  - Missing Energy  $M_E(p e^+ e^-) > 0.075 \text{ GeV}$
  - Kinematic Pull Probabilities
    - $P(\chi^2)$  of  $\gamma p \rightarrow p \pi^+ \pi^- < 1\%$
    - $P(\chi^2)$  of  $\gamma p \rightarrow p e^+ e^- (\gamma) > 1\%$
    - $P(\chi^2)$  of  $\gamma p \rightarrow p e^+ e^- (\gamma) e^+ e^- (\gamma)$  to a  $\pi^0 > 1\%$

# Simulation Verification



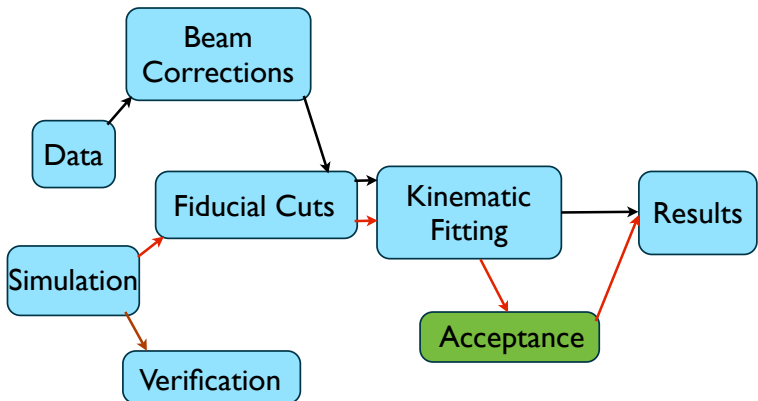
# Simulation Verification

- Simulation efficiency was performed in 2 parts
  - Feeding real data events through simulation chain
  - Generating  $\gamma p \rightarrow p\pi^0$  using SAID differential cross-sections for  $E_\gamma < 2.8$  GeV
  - Generating  $\gamma p \rightarrow p\pi^+\pi^-$  using differential cross-sections for  $E_\gamma < 2.8$  GeV



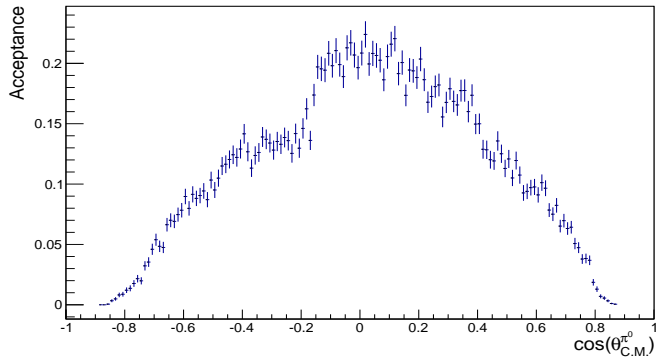
Panel: Comparison of  $e^+e^-$  mass distribution for all MC (black) 124

# Acceptance



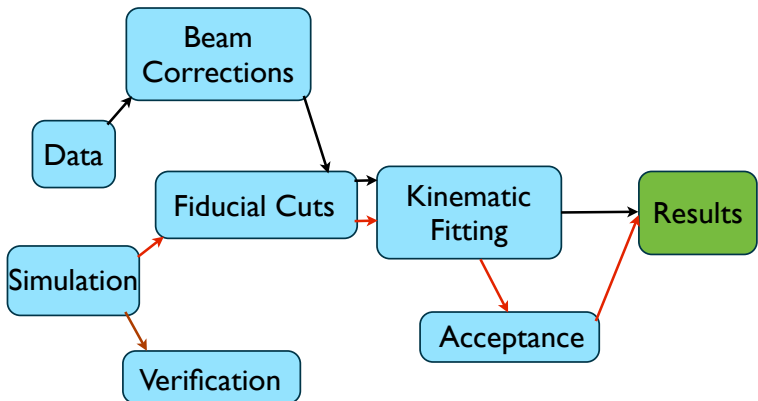
- Acceptance is the efficiency of detecting particles throughout the CLAS detector
- It is calculated as  $\frac{\# \text{reconstructed}}{\# \text{generated}}$  for simulation
- Phasespace generation for  $\gamma p \rightarrow p\pi^0$ 
  - $\pi^0 \rightarrow \gamma\gamma$ 
    - GSIM handled conversion  $\gamma \rightarrow e^+e^-$
  - $\pi^0 \rightarrow e^+e^-\gamma$
- Generated events put through simulation chain
- $\eta(E_\gamma, \cos \theta_{C.M.}^{\pi^0}) = \frac{N_R(E_\gamma, \cos \theta_{C.M.}^{\pi^0})}{N_G(E_\gamma, \cos \theta_{C.M.}^{\pi^0})}$
- Binned in  $E_\gamma$  and  $\cos \theta_{C.M.}^{\pi^0}$ 
  - $E_\gamma$  in 50 MeV bins
  - $\cos \theta_{C.M.}^{\pi^0} = 0.0125$  bins
  - 2.4x finer bins than data

Acceptance at  $E_{\gamma} 4.775 \text{ GeV} \pm 25 \text{ MeV}$



Example of acceptance for one kinematic bin of  $E_{\gamma}$   
 $4.775 \text{ GeV} \pm 50 \text{ MeV}$

## Results

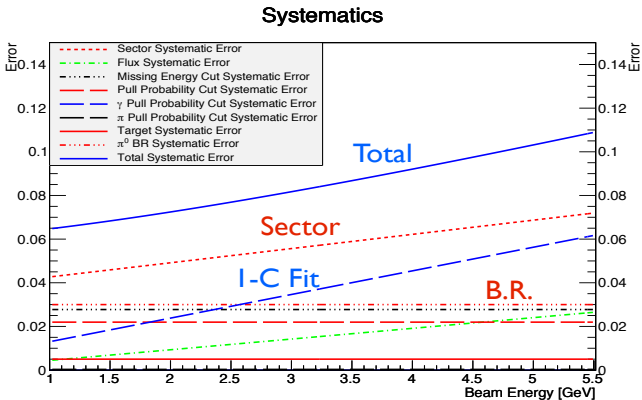


- $$\frac{d\sigma}{d\Omega} = \frac{N_{\pi^0 \rightarrow e^+ e^- \gamma}}{N_{A \pi^0 \rightarrow e^+ e^- \gamma}} \frac{1}{L\rho_t} \frac{1}{\frac{\Gamma_{\pi^0 \rightarrow e^+ e^- \gamma}}{\Gamma_{total}}} \frac{1}{\Delta\Omega}$$
- Where  $N_{A \pi^0 \rightarrow e^+ e^- \gamma}$  is the acceptance for the c.m. angle
- $\frac{\Gamma_{\pi^0 \rightarrow e^+ e^- \gamma}}{\Gamma_{total}}$  is the branching ratio of the dalitz decay
- $L$  is flux
- $\rho_t$  is target density =  $0.0711 \frac{\text{g}}{\text{cm}^3}$  measured
- $\Delta\Omega = 2\pi\Delta\cos\theta$
- $$\frac{d\sigma}{dt} = \frac{\pi}{p_t^* p_p^*} \frac{d\sigma}{d\Omega}$$
, where  $p_t^*$  and  $p_p^*$  are in the C.M. of  $\pi^0$

- 8 total systematics were investigated
  - Branching Ratio Systematic
    - Calculated using known values of B.R. plus  $\gamma$  conversion
  - Target Systematic
    - Determined to be the uncertainty in the length of the target
  - 3 Pull Probability Systematics
    - Determined by varying pulls individually for data and MC and comparing cross-sections
  - Missing Energy Systematic
    - Determined by varying cut for data and MC and comparing cross-sections
  - GFlux Systematic
    - Determined by investigating cross-section and 4 periods in the  $g12$  run
  - Sector Systematic
    - Determined by measuring cross-section in each sector and comparing to sum of all 6 sectors

Table : Systematic errors calculated in  $\frac{d\sigma}{d\Omega}$  measurements

Source	Systematic Error
Sector	$0.0361 + 0.0065E_\gamma$
Flux	$-0.00051 + 0.00491E_\gamma$
Missing Energy Cut	0.02781
$P(\chi^2)$ of 2-C	0.0219
$P(\chi^2)$ of 1-C	$0.00216 + 0.01083E_\gamma$
$P(\chi^2)$ of 4-C	0.00031
Target	0.005
Branching ratio	0.03



Plot showing the contribution of the all systematic errors as well as the combined which was calculated adding all systematic errors in quadrature.

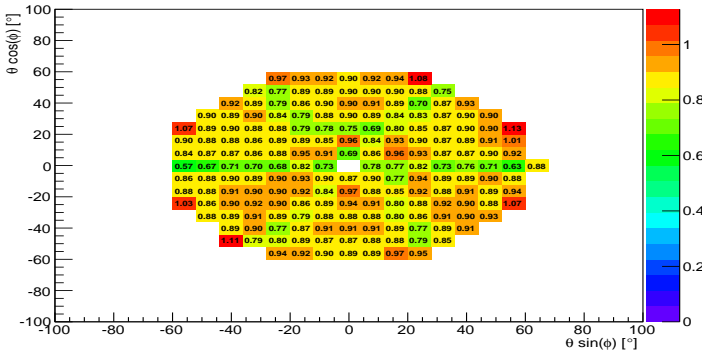
- In the  $g_{11}$  experiment normalization factor was on the order of 18%
- in this analysis,  $g_{12}$ , a normalization constant of 18% was also needed
  - The cause is currently unknown
- GPP is responsible for smearing and dropping inefficient parts of the detector but not trigger efficiency. To investigate this effect the following 3 topologies;
  - $\gamma p \rightarrow p\pi^+(\pi^-)$
  - $\gamma p \rightarrow p\pi^-(\pi^+)$
  - $\gamma p \rightarrow \pi^+\pi^-(p)$

Table : Binning Used in Efficiency Study

z bins [cm] (5 cm increments)	Momentum bins [GeV]
$-70 \text{ cm} < z < -110 \text{ cm}$	<ul style="list-style-type: none"><li>0 - 0.5</li><li>0.5 - 0.75</li><li>0.75 - 1</li><li>1 - 1.5</li><li>1.5 - 2</li><li>2 - 2.5</li><li>2.5 - 3</li><li>3 - 5</li></ul>

## Normalization of Proton

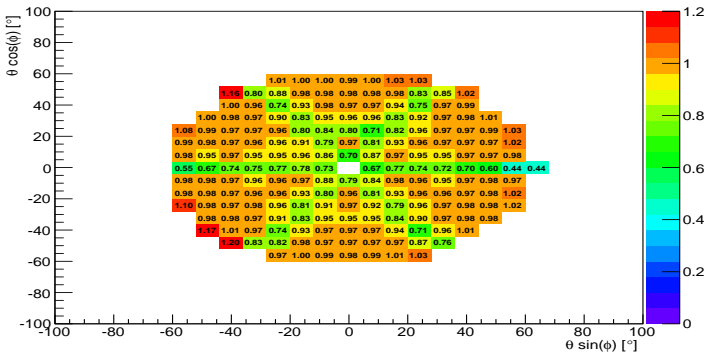
## Proton Data Efficiency at -90. < z < -85. cm at 0.75 < P < 1 GeV



Plot showing the efficiency of detecting the proton for data

# Normalization of Proton

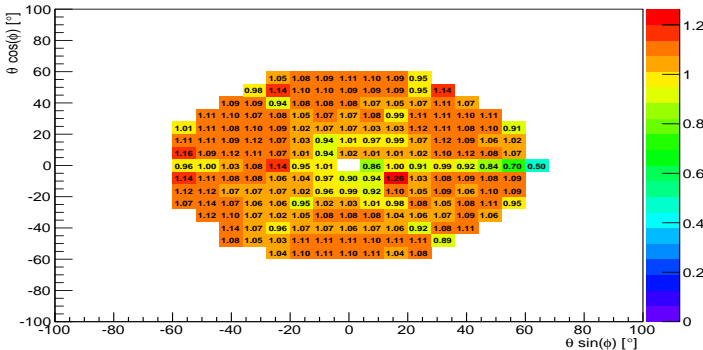
Proton Monte-Carlo Efficiency at  $-90. < z < -85.$  cm at  $0.75 < P < 1$  GeV



Plot showing the efficiency of reconstructing the proton for simulation

# Normalization of Proton

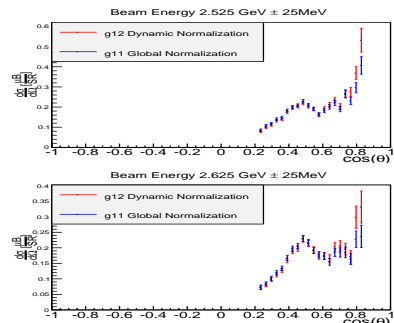
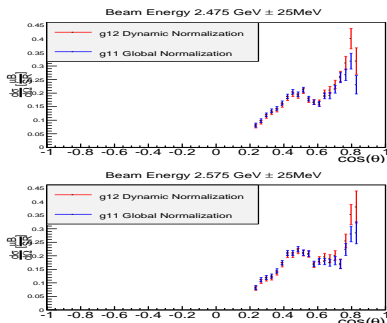
## Proton Over-Efficiency at $-90^\circ \leq z \leq -85^\circ$ , cm at $0.75 \leq P \leq 1$ GeV



Plot showing the over-efficiency of simulating the proton. Ratio of simulation/data

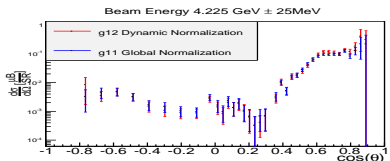
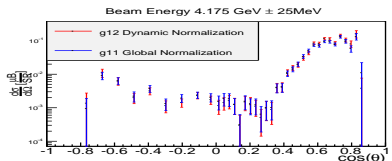
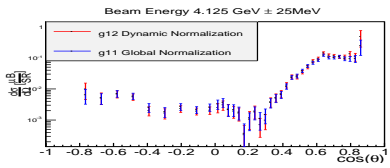
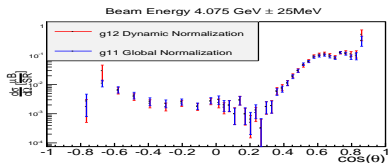
# Effect of Dynamic Normalization

- The same procedure was performed for  $\pi^+$  and  $\pi^-$  events
- Applied combined normalization for each event
  - $\epsilon = \epsilon_{proton} \cdot \epsilon_{\pi^+} \cdot \epsilon_{\pi^-}$
- Compared results to using static 18% normalization

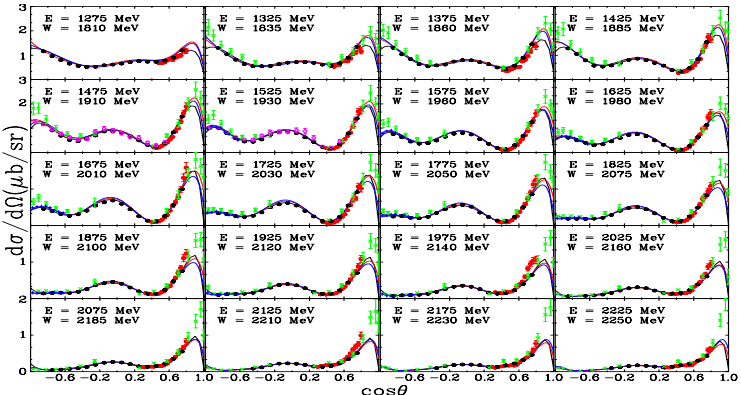


$g12 \pi^0$  differential cross-section when the *g11* global normalization is used and when the *g12* dynamic normalization is used.

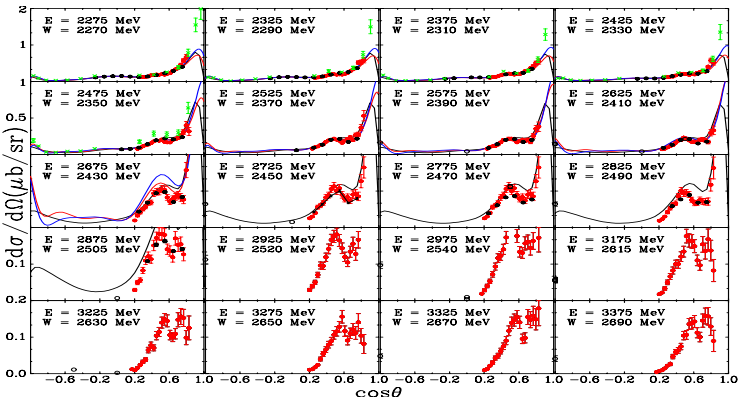
# Effect of Dynamic Normalization



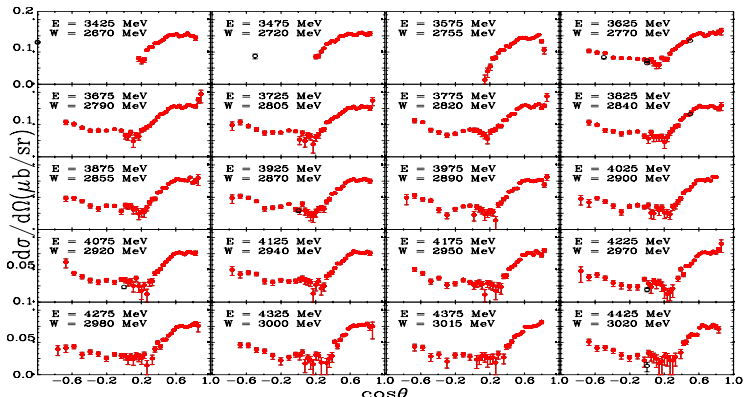
$g12 \pi^0$  differential cross-section when the *g11* global normalization is used and when the *g12* dynamic normalization is used.



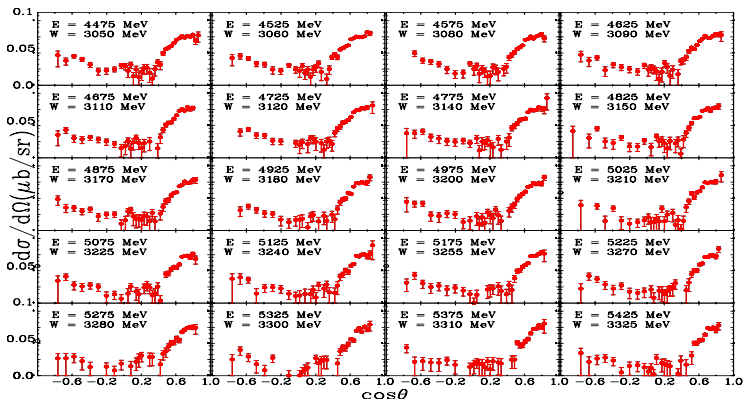
Solid lines SAID KU14 DU13 solution, black solid lines BG2011-02 BnGa predictions. Symbols: **this work**, previous CLAS, **GRAAL**, **LEPS**, **CB-ELSA**, previous bremsstrahlung measurements (black open circles).



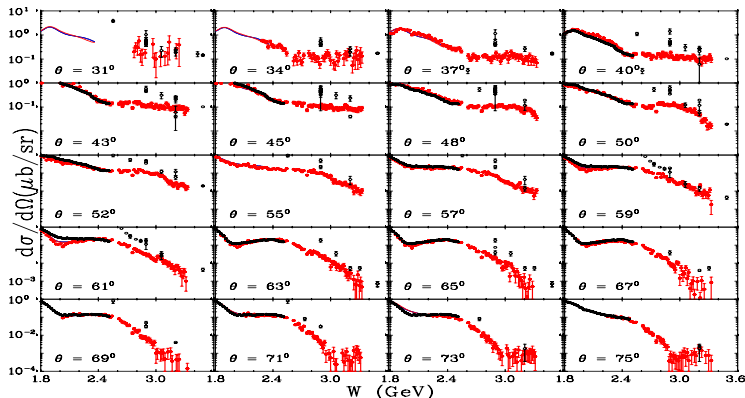
Solid lines SAID KU14 DU13 solution, black solid lines BG2011-02 BnGa predictions. Symbols: **this work**, previous CLAS, **GRAAL**, **LEPS**, **CB-ELSA**, previous bremsstrahlung measurements (black open circles).



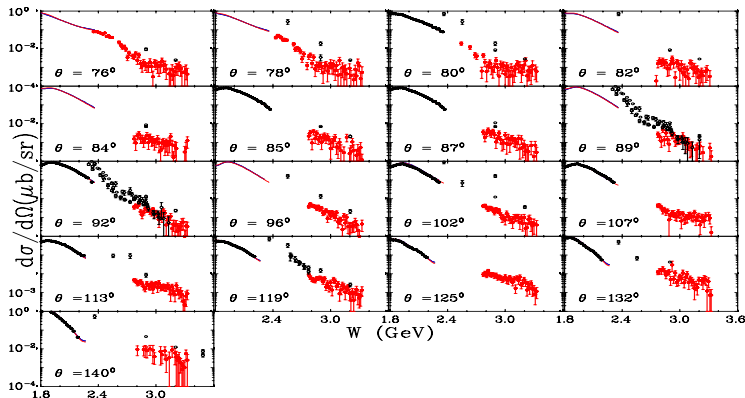
Symbols this work, previous bremsstrahlung measurements  
(black open circles).



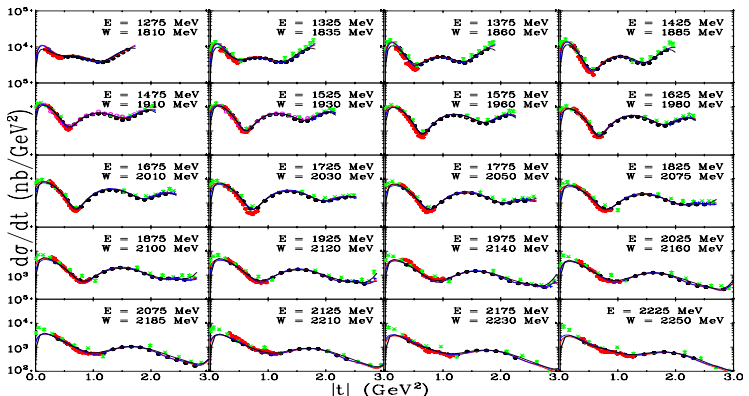
Symbols **this work**, previous bremsstrahlung measurements (black open circles).



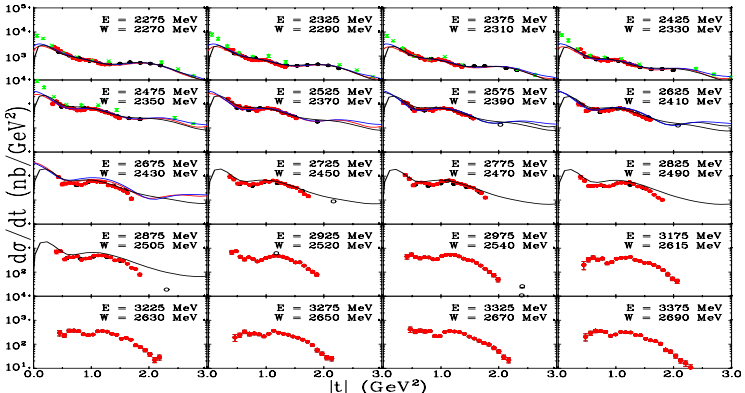
Solid lines SAID KU14 DU13 solution, black solid lines  
BG2011-02 BnGa predictions. Symbols: **this work**, previous  
CLAS, previous bremsstrahlung measurements (black open  
circles).



Solid lines SAID KU14 DU13 solution, black solid lines BG2011-02 BnGa predictions. Symbols: this work, previous CLAS, previous bremsstrahlung measurements (black open circles).

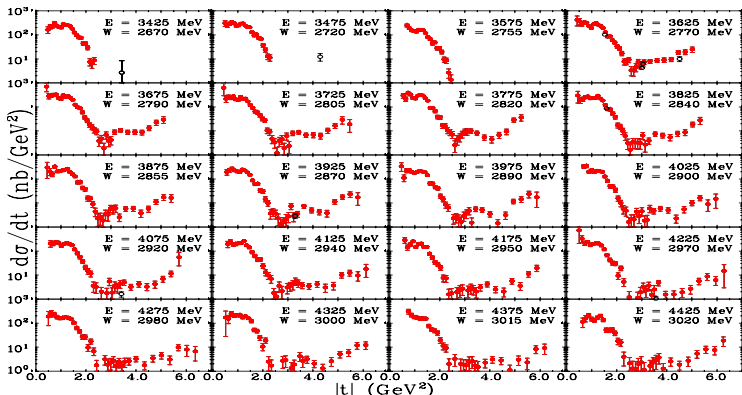


Solid lines SAID KU14 DU13 solution, black solid lines BG2011-02 BnGa predictions. Symbols: this work, previous CLAS, GRAAL, LEPS, CB-ELSA, previous bremsstrahlung measurements (black open circles).



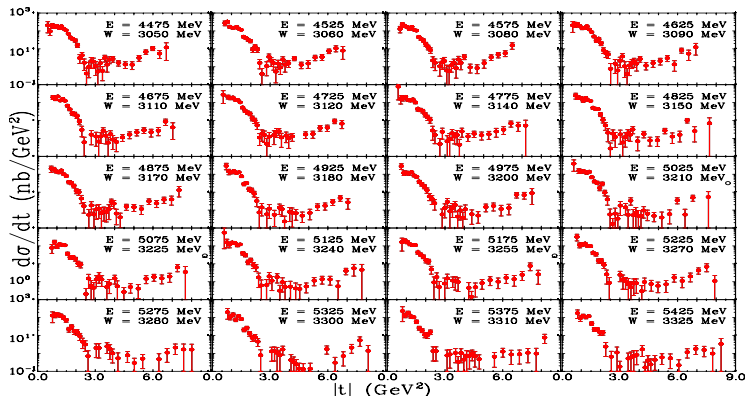
Solid lines SAID KU14 DU13 solution, black solid lines  
BG2011-02 BnGa predictions. Symbols; **this work**, previous  
CLAS, **GRAAL**, **LEPS**, **CB-ELSA**, previous bremsstrahlung  
measurements (black open circles).

**$t$  vs.  $d\sigma/dt$  at  $E_\gamma = 3425 - 4425$  MeV**



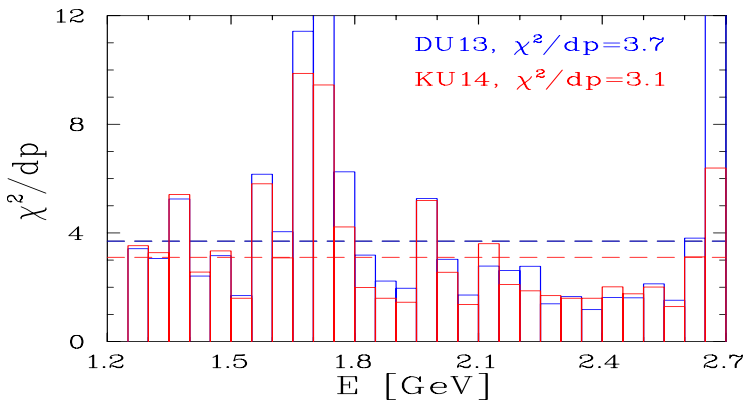
Symbols this work, previous bremsstrahlung measurements  
(black open circles).

$t$  vs.  $d\sigma/dt$  at  $E_\gamma = 4475 - 5425$  MeV



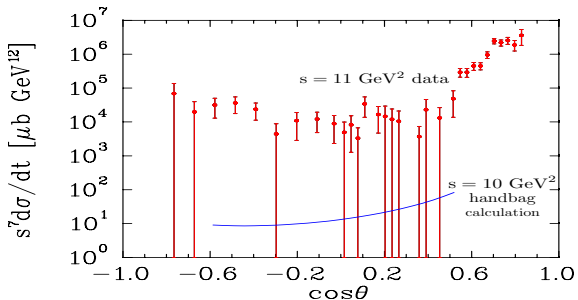
Symbols this work, previous bremsstrahlung measurements (black open circles).

## Improvement to Previous SAID Fits



Energy dependence of the  $\chi^2/dp$  comparison to previous SAID fits, previous DU13 solution, compared to the new KU14 solution.

## Comparison with GPD Handbag Model



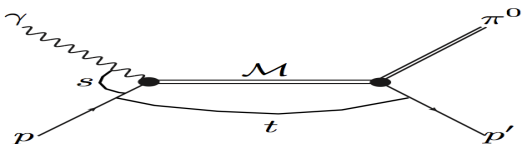
Differential cross section of  $\pi^0$  photoproduction.  $E_\gamma = 5.4 \text{ GeV}$  for  $s = 11 \text{ GeV}^2$ .  $E_\gamma = 4.8 \text{ GeV}$  for  $s = 10 \text{ GeV}^2$   
Based on this data, a proposal was approved to run in Hall C

## Summary and Conclusions

- We measured  $\pi^0$  photoproduction for  $\gamma p \rightarrow p\pi^0 \rightarrow pe^+e^-\gamma$
- Data corrections, kinematic fitting and fiducial cuts were used to clean the data  $\approx 99\%$
- This data set explained in this analysis is 10% of the world data for  $\pi^0$  photoproduction
- More theory is needed to properly explain  $\pi^0$  production at incident photon beam energies higher than 2.8 GeV
- Differential cross-sections  $\frac{d\sigma}{d\Omega}$  and  $\frac{d\sigma}{dt}$ , were compared to world data
- Agreed well  $E_\gamma < 2.8$  GeV
- The fits using the SAID parametrization yielded a  $\chi^2/dp$  lower than previous existing fits
- Handbag calculations do not reproduce data for  $E_\gamma > 2.8$  GeV
- Analysis note + paper currently in progress

- Extras are after this →

- Provide insight into the mechanisms, baryon resonances and production channels involved in  $\pi^0$  production
  - For incident beam energies already explored previously as well as for incident beam energies in which there exists only a sparse and in some cases no amount of data
- Recently there has been improvement in Wide Angle Compton Scattering predictions using a Generalized Parton Distribution (GPD) handbag model.
  - This framework has also been recently adopted into  $\pi^0$  production
  - The production of the nucleons is considered in a 2 part soft and hard mechanism exchange
- Goal is to provide precise measurements of the  $\pi^0$  cross-section
  - Compare to existing data
  - Check validity of handbag model



$$\begin{aligned} \mathcal{M} = & \left[ \frac{1}{2} i \gamma_5 \gamma_\mu \gamma_\nu A_1(s, t) + 2 i \gamma_5 P_\mu \left( q - \frac{1}{2} k \right)_\nu A_2(s, t) \right. \\ & \left. + \gamma_5 \gamma_\mu q_\nu A_3(s, t) + \gamma_5 \gamma_\mu (2P_\nu - iM\gamma_\nu) A_4(s, t) \right] (\epsilon_\mu k_\nu - \epsilon_\nu k_\mu) \end{aligned}$$

- $q_\mu$  and  $k_\nu$  are the four-momenta of the  $\pi^0$  and photon respectively
- $P_\mu = \frac{1}{2}(p_{1\mu} + p_{2\nu})$
- $\epsilon_\mu \equiv$  photon polarization

- The  $\pi^0$  cross-section can be reconstructed by electric ( $E_{l\pm}$ ) and magnetic ( $M_{l\pm}$ ) multipole amplitudes
  - $l$  is angular momentum of the final state with total angular momentum  $j = l \pm \frac{1}{2}$
- Isospin Decomposition
  - The photon interaction has an isovector part and isoscalar part
  - The isovector photon produces final states with isospin  $\frac{3}{2}$  and  $\frac{1}{2}$  with amplitudes  $A^{V3}$  and  $A^{V1}$
  - The isoscalar photon gives final states of isospin  $\frac{1}{2}$  with amplitude  $A^S$ .
  - $\pi^0 : A^0 = \sqrt{\frac{2}{3}}A^{V3} + \sqrt{\frac{1}{3}}(A^{V1} - A^S)$
- Helicity Partial-Wave Amplitudes
- CGLN Amplitudes

- $\pi^0$  production is factorized into two parts
  - one quark from the incoming and one from the outgoing nucleon participate in the hard sub-process (small blob)
    - calculable using PQCD
  - The soft part consists of all the other partons that are spectators and can be described in terms of GPDs (large blob)

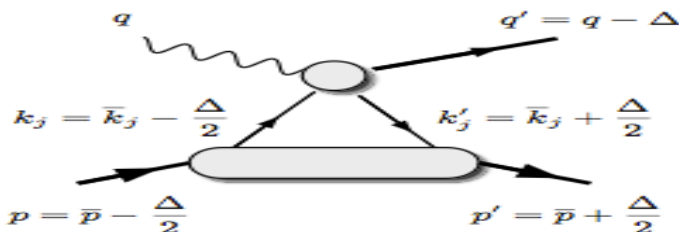
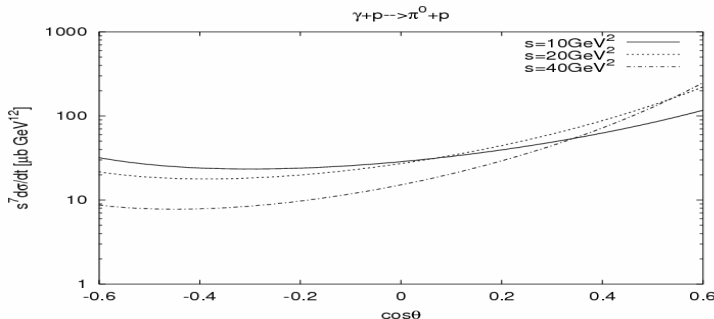


Figure : The handbag-type diagram for photoproduction of mesons.

# $\pi^0$ Production above 2.8 GeV

- Recent framework of handbag model led to  $\pi^0$  cross-section predictions



**Figure :** The soft physics contribution to the cross-section for photoproduction of  $\pi^0$  scaled by  $s^7$  versus  $\cos\theta$ , where  $\theta$  is the scattering angle in the  $\gamma p$  c.m. system.

- SAID is a repository of experimental data and an interactive analysis facility
  - Allows to compare and extract data and partial wave solutions (PWA) for a variety of photoproduction, electro-production and pion production reactions
- SAID generates resonance couplings, in terms of angular momentum and isospin quantum numbers
  - Extracted from a fit-based determination of multipoles using both an energy-dependent and an energy-independent parametrization

- The  $\pi^0$  decays to 2 photons  $98.823 \pm 0.034\%$ 
  - Each photon has equal probability of pair producing  $e^+e^-$  pairs
- The  $\pi^0$  decays to  $e^+e^- \gamma$   $1.174 \pm 0.035\%$

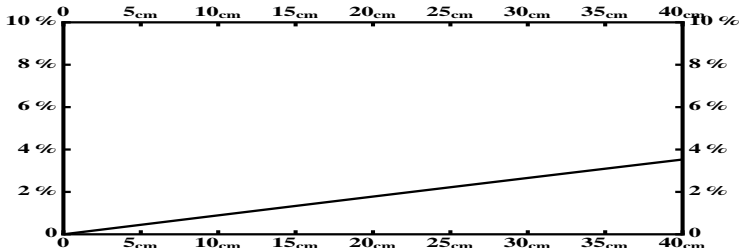


Figure : Probability of pair production,  $\gamma \rightarrow e^+e^-$ , in 40 cm of liquid hydrogen.

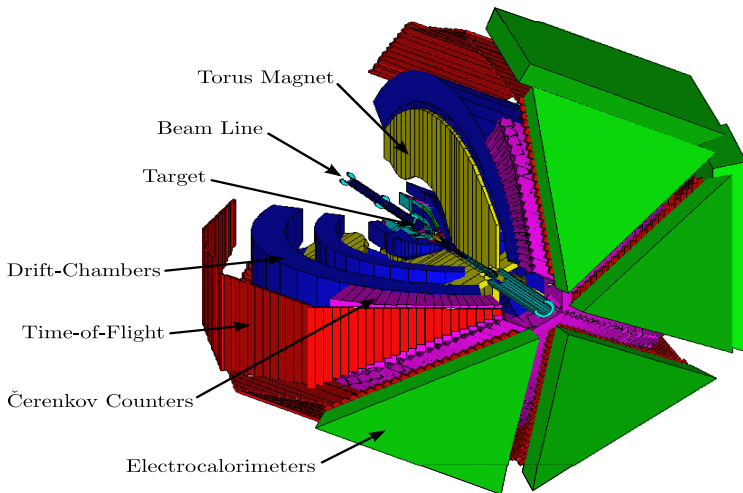


Figure : CLAS Detector with labeling

- Bremsstrahlung photon beam
  - $e^-$  beam of 5.7 GeV
  - gold radiator  $10^{-4}$  radiation lengths
  - Tagged  $\gamma$  energies  $1.1 \rightarrow 5.5$  GeV
  - 6.2 mm diameter collimator 537 cm before  $\ell H_2$  target

- Liquid Hydrogen  $\ell H_2$  Target
  - Unpolarized
  - 40 cm in length
  - 2 cm radius
    - $\gamma$  beam had 1.5 cm radius exiting  $\ell H_2$  target
  - Placed 90 cm upstream from CLAS center
    - Geometric acceptance of 6° instead of 8° in lab frame
    - Geometric acceptance of 100° instead of 140° in lab frame

- CC's were filled with perflourbutane  $C_4F_{10}$ 
  - Index of refraction 1.0015
  - $\pi^\pm$  threshold of 2.7 GeV
  - $e^\pm$  threshold of 9 MeV
  - $e^\pm$  detection efficiency > 97% for charged particles below 2.5 GeV.

- $e^\pm$  trigger
  - Single track  
(ST\*TOF)\*(EC\*CC)
  - L2 multiplicity of 2.
    - 2 tracks were detected in the Drift Chambers
  - Trigger bit was set to be 6 of 12

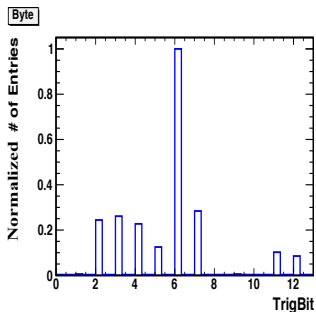


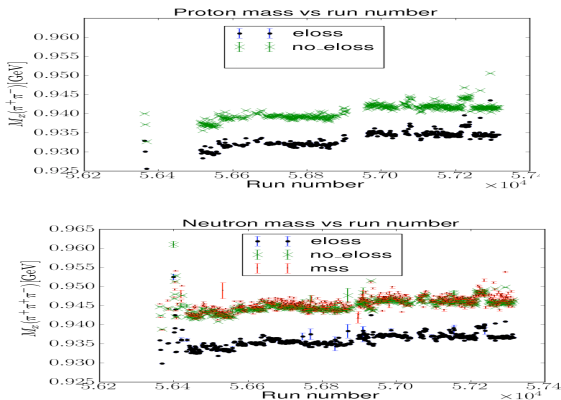
Figure : Triggers fired for leptons

- Data was taken in Hall B experiment G12
- Running Time: 04/2008 → 06/2008
- 44 Days of Beam Time
- 60 - 65 nA of current
- $E_\gamma$  up to 5.5 GeV
- 126 TB Raw Data
- Raw sensitivity of  $53 \text{ pb}^{-1}$
- $26.2 \times 10^9$  production triggers ( $3 \times 10^6$  di-lepton triggers)
- EC and CC combine to provide an  $e/\pi$  rejection factor of  $10^{-6}$  for di-lepton pairs.
- $$\frac{\Gamma_{e^+ e^- \gamma}}{\Gamma_{\pi^+ \pi^- \gamma}} = 0.237 \pm 0.026$$

- Tracking begins after the particle had already traversed through the target and ST
  - Momentum determination was skewed by the “energy-loss” the particle underwent before entering Region 1
  - “Energy-loss’ is due to charged particles losing their energy through atomic excitation and ionization while traveling through materials in the CLAS detector
  - Leptons such as electrons/positrons or muons are not subjective to “energy-loss”.
- Eloss software package written by Eugene Pasyuk for the CLAS detector has been implemented in this analysis

# Beam Corrections

- First noticed by *g12* participants at the analysis level in which  $M_x(\pi^+\pi^-)$  and  $M_x(\pi^+\pi^-\pi^+)$  masses were systematically low. Varied in mass as much as 10 MeV.
- Dependent on the run number



- Investigated invariant mass of  $M(\pi^+\pi^-) = M_{K_s}$  for run number dependence
  - Dependent on the run number was not found

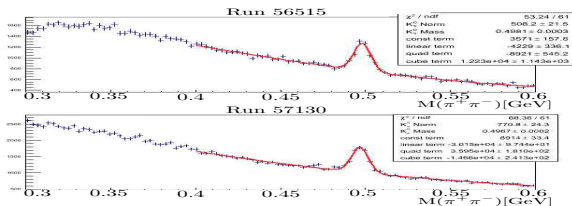


Figure : Plot of Kaon mass for runs 56515 and 57130. PDG mass for the kaon is 0.497614 GeV/c.

- Problem was associated with the beam
- Tagger y-dump positioning changed
  - *g12* performed shut down midway. Upon restart the tagger magnet was also restarted

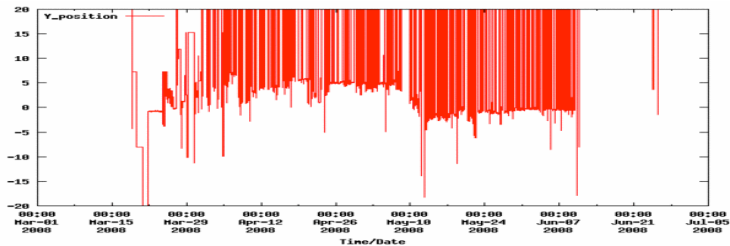
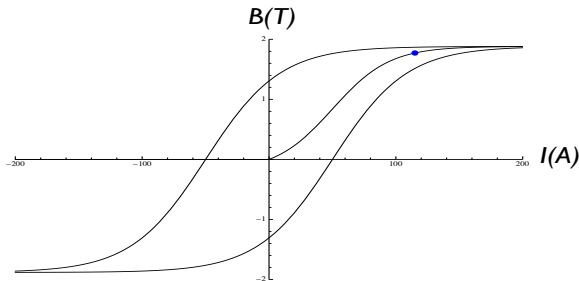


Figure : Tagger dump y-positioning according to EPICS

- Problem identified as hysteresis in the tagger magnet



**Figure :** Plot depicting the process of hysteresis. For a current of strength  $I$ , there could exist two magnetic fields of strength  $B$ .

- $(P_\gamma + P_{target} - (P_{\pi^+ \pi^-}))^2 = m_p^2$
- $P_{\pi^+ \pi^-}^2 - 2P_{target}P_{\pi^+ \pi^-} = 2P_\gamma(P_{\pi^+ \pi^-} - P_{target})$
- $P_\gamma = P_{E_0} - P_e$ 
  - $P_{E_0}$  beam energy delivered from CEBAF
  - $P_e$  scattered electron in the *bremsstrahlung* process that is recorded by the tagger
- Correction factor
  - $x = \frac{P_{E_0}(P_{target} - P_{\pi^+ \pi^-}) + P_{\pi^+ \pi^-}^2 / 2 - P_{target}P_{\pi^+ \pi^-}}{(P_{E_0} - P_\gamma)(P_{target} - P_{\pi^+ \pi^-})}$
  - $P_\gamma^{new} = P_{E_0} - P_e * x$

## Beam Correction

- Value of x was obtained for each run
- Applied correction to the topology  $\gamma p \rightarrow \pi^+ \pi^+ \pi^- (n)$

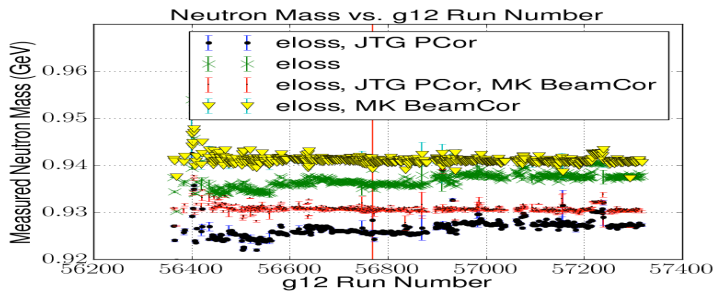


Figure : Plot of missing neutron mass using various corrections.

# Geometric Fiducial Cuts

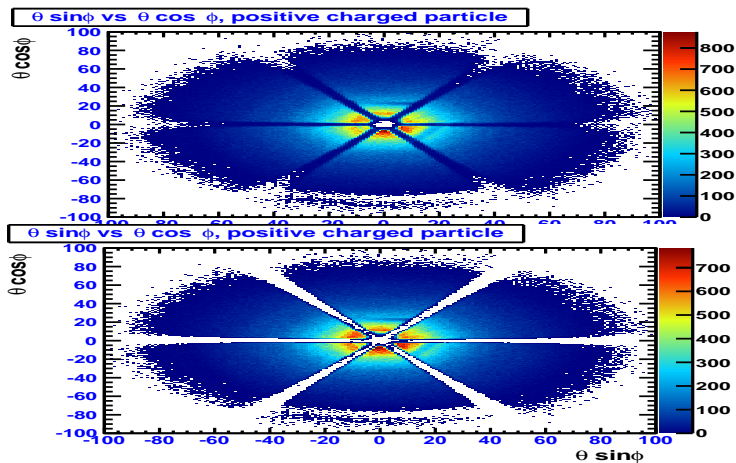


Figure : Positive charged tracks in CLAS DC before and after fiducial cut being applied

# Geometric Fiducial Cuts

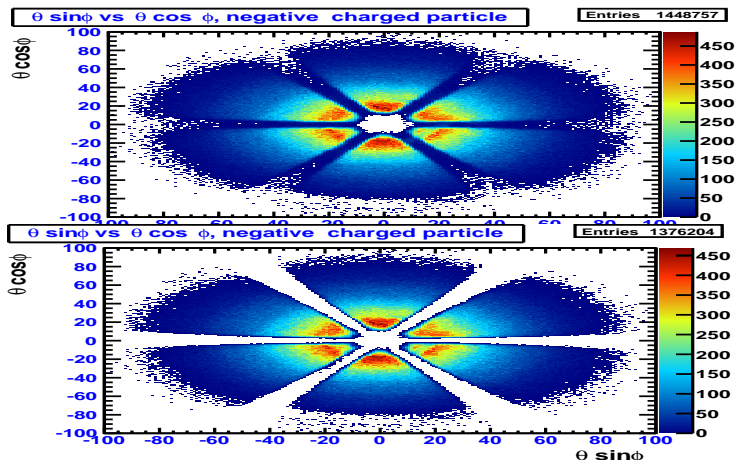


Figure : Negative charged tracks in CLAS DC before and after fiducial cut being applied

- EC dead/inefficient PMT's were found and removed

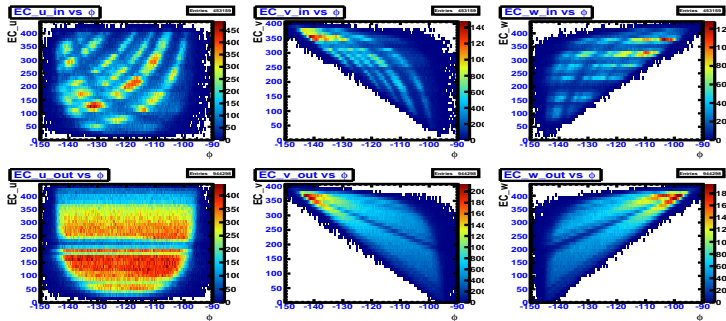


Figure : Inefficiency seen in CLAS  $e^-$  data, due to an inefficient EC strips. Top row depicts the U, V, W strips for the *inner* EC, while the bottom row depicts the U, V, W strips for the *outer* EC

- EC sectors 1, 2, 3, 5 had dead/inefficient PMT's. Sector 5 was the worst

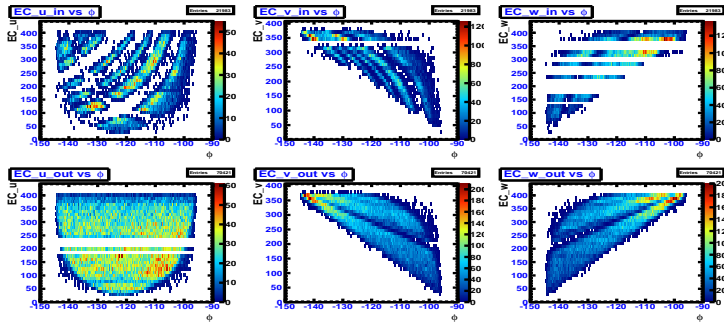


Figure : Plot depicting fiducial cuts and inefficient paddle knockouts applied to  $e^-$  data. Top row depicts the U, V, W strips for the *inner* EC, while the bottom row depicts the U, V, W strips for the *outer* EC

## TOF Fiducial Cuts

- Sector 1 and 3 had dead/inefficient TOF paddles
- Performing a geometric cut on is same as cutting dead paddles

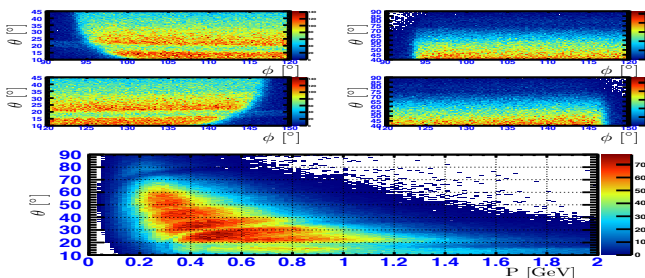


Figure : Inefficiency seen in CLAS  $\pi^+$  data, due to an inefficient TOF paddle.

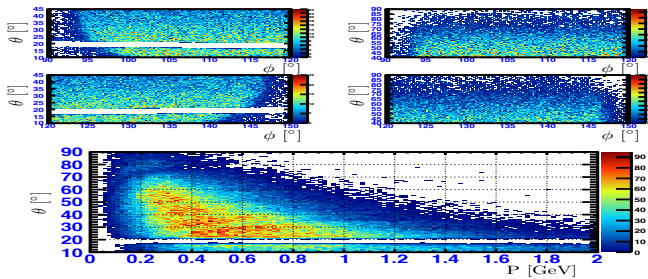


Figure : Inefficiency cut for  $\pi^+$  and proton data.

- Simulation Chain

- PLUTO++ as generator
- GAMP2PART
- GSIM
- GPP
- A1C
- ANALYSIS CODE

- Lepton triggered was simulated by
  - The sector with the highest EC summed energy over threshold.
  - The sector with the highest EC Inner Layer summed energy over threshold.
  - The sector with the highest CC summed energy over threshold.
  - All three above conditions must be in same sector.
- This procedure is how data is triggered in *g12*
- Simulating the trigger in conjunction with cc and EC hit requirements reduced the yield of the simulation to 69.48% while for the data the reduction is 69.91%

## Simulation Verification

- Real data was inputted into GSIM
- Initially had success rate of 0.75% due to GSIM CC and EC pedestal values at reconstruction
- A special CLAS\_CALDB\_RUNINDEX was created for leptons and photons after which  $\approx 95\%$  success
- Missing 5% is start-counter failure seen in both MC and data due to sector random bug

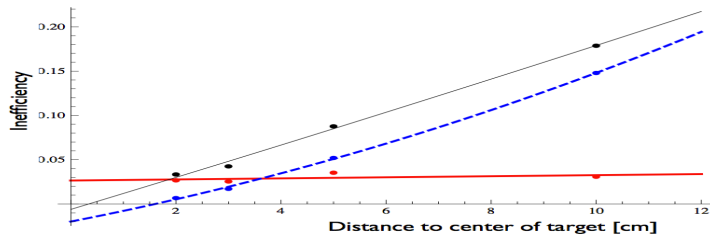


Figure : Start counter inefficiency

- $\eta = y + \epsilon$ 
  - Use of Lagrange multipliers and least-squares fitting
- $P(\chi^2) = \int_{\chi^2}^{\infty} f(x, n) dx$ 
  - $f(x, n) \equiv \chi^2$  probability density function for  $n$  degrees of freedom
  - $0 < P(\chi^2) < 1$
- $\vec{z} = \frac{\vec{\eta}_i - \vec{\eta}_f}{\sqrt{\sigma_{\vec{\eta}_i}^2 - \sigma_{\vec{\eta}_f}^2}}$

# Kinematic Fitting

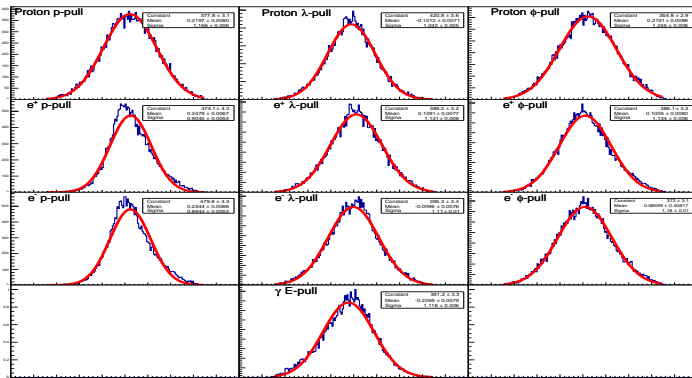


Figure : Pull distribution for the (4-C) kinematic fit for  $\gamma p \rightarrow pe^+e^-$  for  $g_{12}$  data with a 1% Confidence Level cut applied, and a Gaussian fit to each.

# Kinematic Fitting

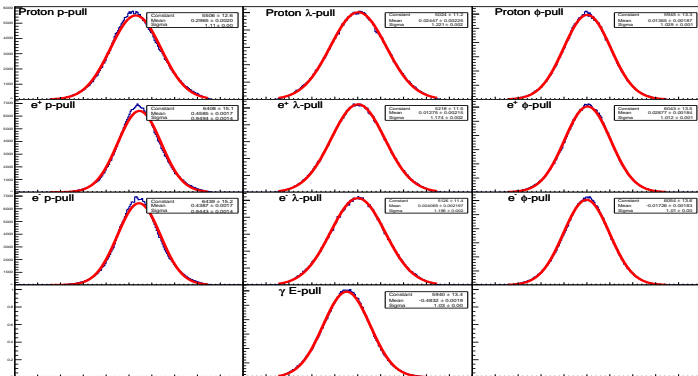


Figure : Pull distribution for the (4-C) kinematic fit for  $\gamma p \rightarrow pe^+e^-$  for  $g12$  simulation with a 1% Confidence Level cut applied, and a Gaussian fit to each.

# Kinematic Fitting

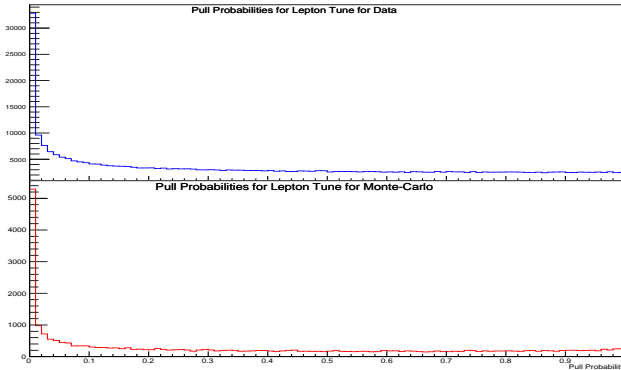


Figure : Confidence Level for  $g_{12}$  (top) data and  $g_{12}$  simulation (bottom) for a (4-C) fit using  $\gamma p \rightarrow pe^+e^-$

# Kinematic Fitting

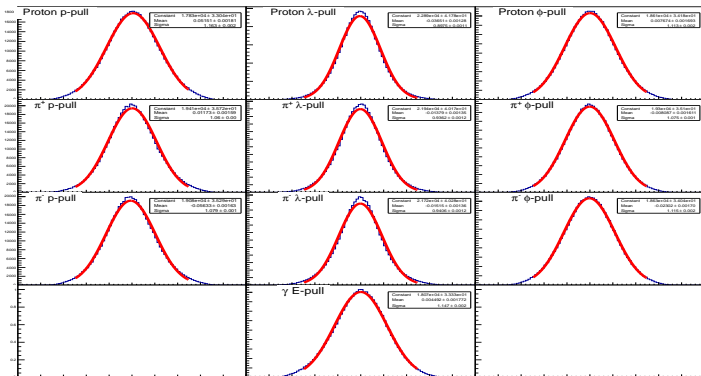


Figure : Pull distribution for the (4-C) kinematic fit for  $\gamma p \rightarrow p\pi^+\pi^-$  for  $g_{12}$  data with a 1% Confidence Level cut applied, and a Gaussian fit to each.

# Kinematic Fitting

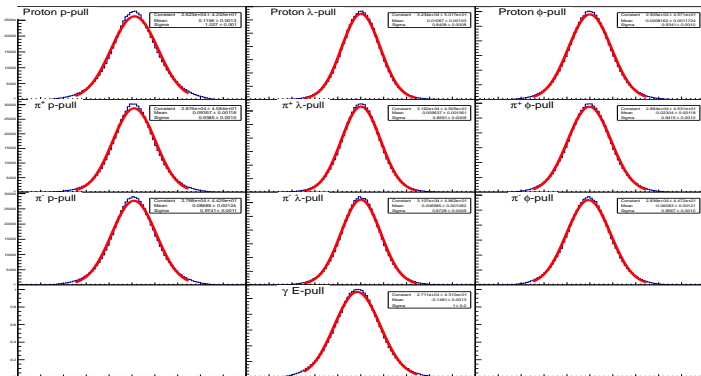


Figure : Pull distribution for the (4-C) kinematic fit for  $\gamma p \rightarrow p\pi^+\pi^-$  for  $g_{12}$  simulation with a 1% Confidence Level cut applied, and a Gaussian fit to each.

# Kinematic Fitting

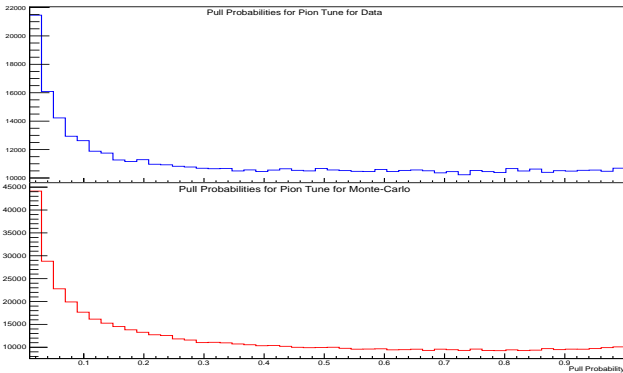


Figure : Confidence Level for  $g_{12}$  (top) data and  $g_{12}$  simulation (bottom) for a (4-C) fit using  $\gamma p \rightarrow p\pi^+\pi^-$

- This analysis performed three separate kinematic fitting hypotheses, 4-C, 1-C and 2-C
  - The 4-C fit was used to the topology of  $\gamma p \rightarrow p\pi^+\pi^-$  to filter background from double charged pion production from single  $\pi^0$  production.
  - The 1-C fit was used to the topology of  $\gamma p \rightarrow pe^+e^-(\gamma)$  to fit to a missing final state photon
  - The 2-C fit was used to the topology of  $\gamma p \rightarrow pe^+e^-(\gamma)$  to fit to a missing final state photon but also fitting  $e^+e^-(\gamma)$  to a  $\pi^0$

# Kinematic Fitting

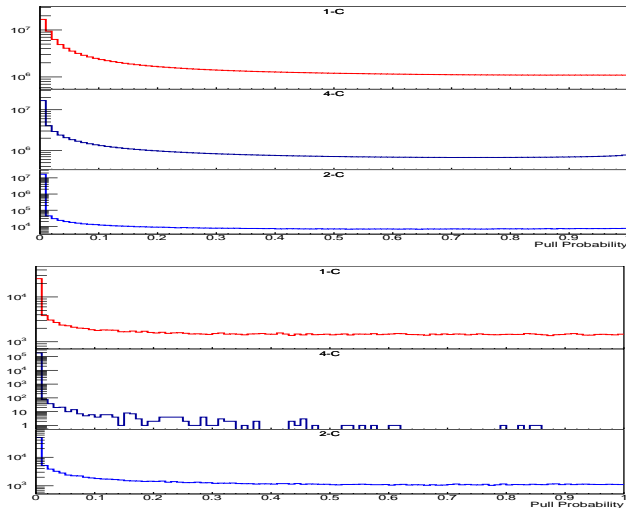
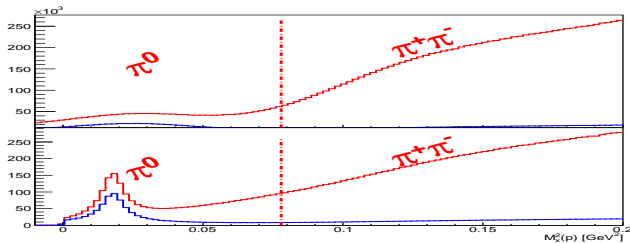


Figure : Pull distribution for the 1-C(red), 4-C(black), 2-C(blue) for  $g_{12}$  data (top) and MC(bottom)

# Kinematic Fitting



**Figure :** Effect of kinematic fitting, on data, prior to cuts for beam energies below 3.6 GeV. The top panel depicts the unfitted data, where the red data line represents all data while the blue line depicts all data with cuts placed on CC and EC hits to be present. The bottom panel depicts the data output from the kinematic fitter 1-C fit, where the red data line represents all data while the blue line depicts all data with cuts placed on CC and EC hits to be present.

# Kinematic Fitting

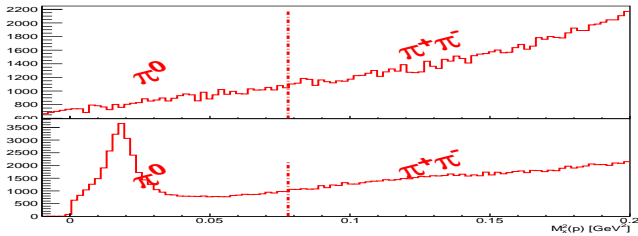
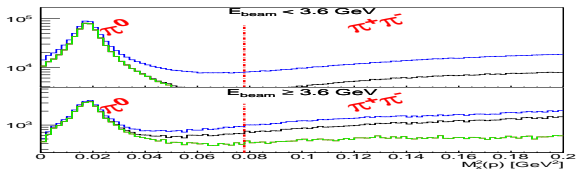
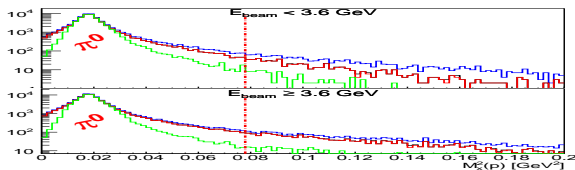


Figure : Effect of kinematic fitting, on data, prior to cuts for beam energies above 3.6 GeV. The top panel depicts the unfitted data. The bottom panel depicts the data output from the kinematic fitter 1-C fit.

# Kinematic Fitting Cuts



(a)



(b)

**Figure :** Mass squared distributions of  $\gamma p - p$ . Blue lines depict the fitted data prior to topological cuts, black line depicts after a 1% cut placed on the 1-C and green line depicts the effect of the 1% 4-C fit cut. Top panel depicts data while bottom panel depicts MC.

# Kinematic Fitting Missing Energy

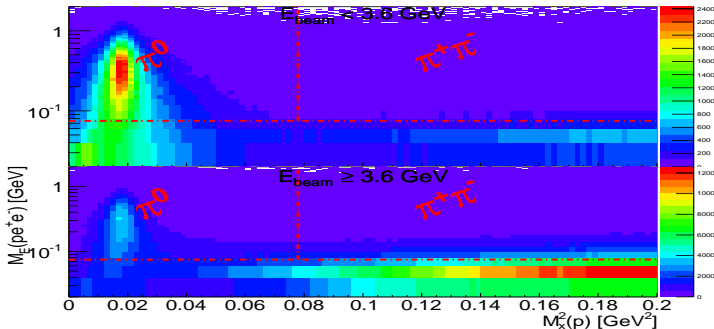


**Figure :**  $M_x^2(p)$  vs.  $M_E^2(pe^+e^-)$ . The horizontal red dashed-dotted line depicts the 75 MeV cut used in this analysis. The vertical red dashed-dotted line depicts boundary of single  $\pi^0$  to  $\pi^+\pi^-$  production.

# Kinematic Fitting 1C and 4C Cuts

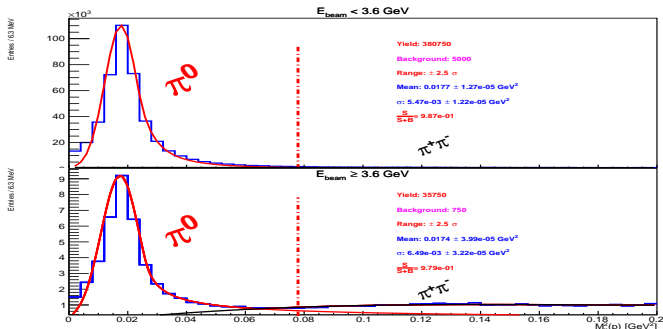
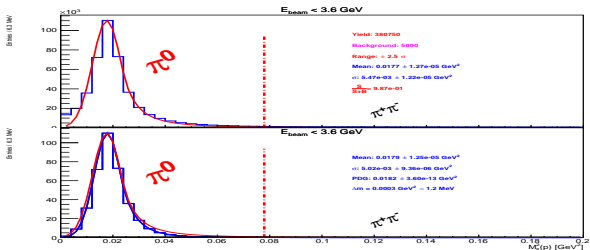


Figure :  $M_x^2(p)$  distribution after the 1-C, 4-C and 75 MeV missing energy cut. Top plots illustrates events with beam energies less than 3.6 GeV, while the bottom plot illustrates events with beam energies greater than 3.6 GeV. The red solid line are fits using the *Crystal Ball Function*, while the black line illustrates the 3<sup>rd</sup> order polynomial background function.

# Kinematic Fitting 2C Cut



- $t_{vert} = t_{TOF} - l_{TOF}/(c\beta)$ 
  - $t_{TOF}$  and  $l_{TOF}$  are the time and length measurement, respectively
  - $\beta = \frac{p}{E} = \frac{p}{\sqrt{p^2+m^2}}$  from DC
- Another means of calculating timing
- $t_{vert} = t_{pho} + t_{prop}$ 
  - $t_{pho}$  is the RF-corrected time that the photon crossed the center of the target
  - $t_{prop}$  is the propagation time from the center of the target to the track's vertex z-coordinate
- Compare the 2 values of timing for accurate mass determination
- Cut of 1.2 ns was used

# Timing

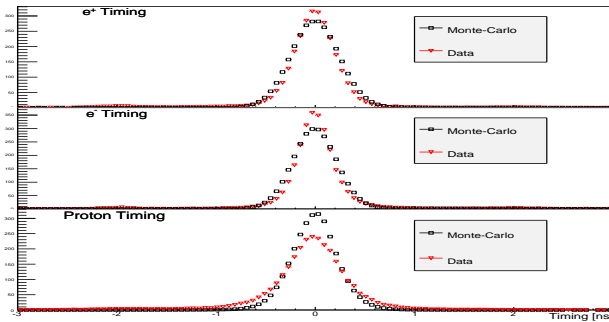


Figure : Timing comparisons of MC and data for proton,  $e^-$ , and  $e^+$

## Simulation Kinematic Verification

- To verify if GSIM simulates *pair-production* properly and other kinematic variables, PLUTO++ in conjunction with SAID cross-sections for  $\pi^0$  and Durham database for  $\pi^+\pi^-$  cross-section was used to generate the expected amount of events of  $\pi^0$  and  $\pi^+\pi^-$

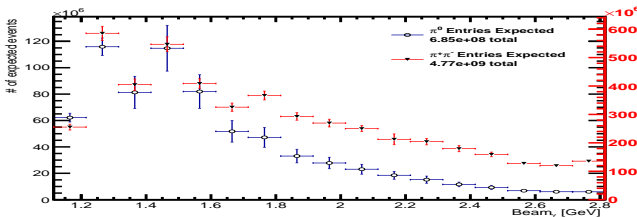
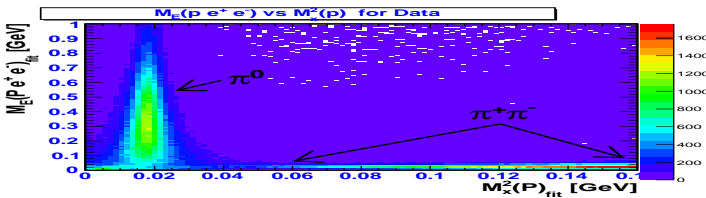
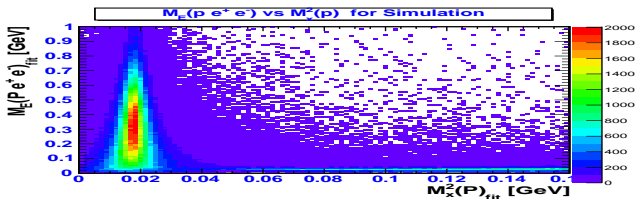


Figure : Total Number of  $\pi^0$  (black open circles) and  $\pi^+\pi^-$  (black closed triangles) events expected between  $E_\gamma$  1.1 GeV-2.8 GeV. The left axes depicts the events expected for  $\pi^0$  production while the right axes depicts the events expected from  $\pi^+\pi^-$  production.

# Simulation Kinematic Verification



(a)



(b)

Figure : M<sub>x</sub><sup>2</sup>(p) vs. M<sub>E</sub><sup>2</sup>(pe<sup>+</sup>e<sup>-</sup>). Top panel(a) depicts data, while the bottom panel (b) depicts MC.

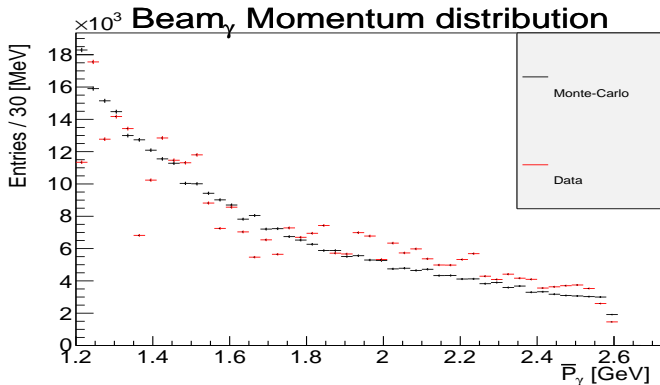


Figure : Comparison of incident photon beam kinematics for MC (black) events and data (red) when generating MC via differential cross-sections. Normalization factor is 1.011.

# Simulation Kinematic Verification

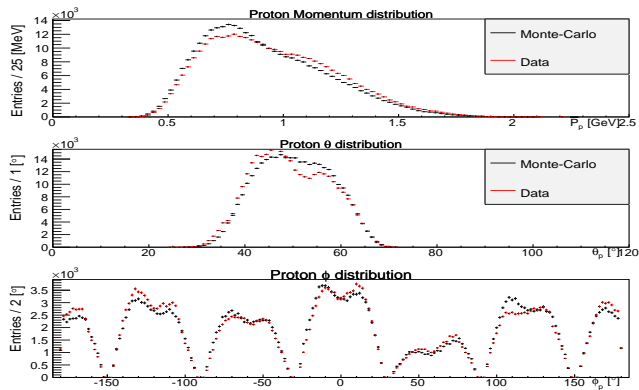


Figure : Comparison of proton kinematics for MC (black) events and data (red) when generating MC via differential cross-sections. Normalization factor is 1.011.

# Simulation Kinematic Verification

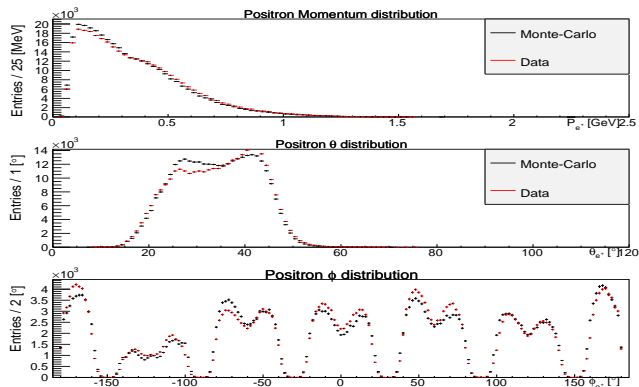


Figure : Comparison of positron kinematics for MC (black) events and data (red) when generating MC via differential cross-sections. Normalization factor is 1.011.

# Simulation Kinematic Verification

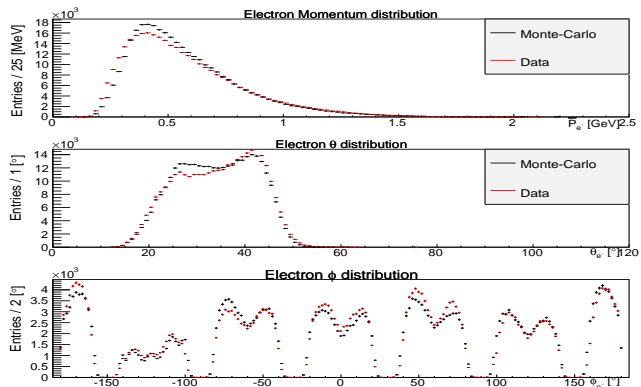


Figure : Comparison of electron kinematics for MC (black) events and data (red) when generating MC via differential cross-sections. Normalization factor is 1.011.

# Simulation Kinematic Verification

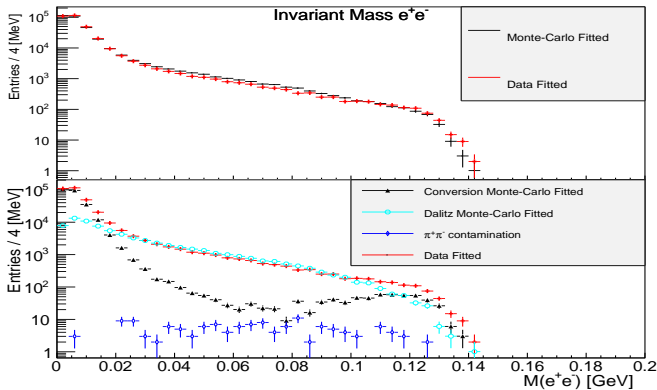


Figure : Top Panel: Comparison of  $e^+e^-$  mass distribution for all MC (black) events and data (red). Bottom Panel: Sources of the MC  $e^+e^-$  topology overlaid to the data. Normalization factor is 1.011.

# Final $\pi^0$ Mass Spectrum

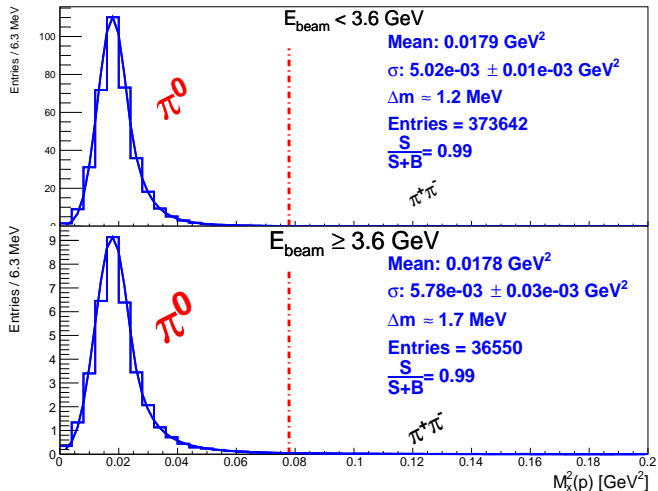


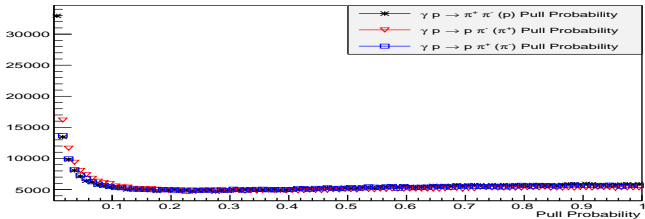
Figure : Final  $M_x^2(p)$  data used in analysis.

- $$\frac{d\sigma}{d\Omega} = \frac{N_{\pi^0 \rightarrow e^+ e^- \gamma}}{N_{A \pi^0 \rightarrow e^+ e^- \gamma}} \frac{1}{L\rho_t} \frac{1}{\frac{\Gamma_{\pi^0 \rightarrow e^+ e^- \gamma}}{\Gamma_{total}}} \frac{1}{\Delta\Omega}$$
- Where  $N_{A \pi^0 \rightarrow e^+ e^- \gamma}$  is the acceptance for the c.m. angle
- $\frac{\Gamma_{\pi^0 \rightarrow e^+ e^- \gamma}}{\Gamma_{total}}$  is the branching ratio of the dalitz decay
- L is flux
- $\rho_t$  is target density =  $(2. / 2.01588) \cdot 0.0717 \cdot 40. \cdot 6.022e23$
- $\Delta\Omega \cdot 2\pi \Delta\cos\theta$

- In the  $g_{11}$  experiment normalization factor was on the order of 18%
- in this analysis,  $g_{12}$ , a normalization constant of 18% was also needed
  - The cause is currently unknown
- GPP is responsible for smearing and dropping inefficient parts of the detector but not trigger efficiency, therefore the normalization could be simulated if it was a trigger effect or another happenstance related to requiring 3 charged tracks in the analysis. To investigate this effect the following 3 topologies;
  - $\gamma p \rightarrow p\pi^+(\pi^-)$
  - $\gamma p \rightarrow p\pi^-(\pi^+)$
  - $\gamma p \rightarrow \pi^+\pi^-(p)$

# Normalization

Pull Probabilities for Normalization Study



Pull Probabilities for Normalization Study for Monte-Carlo

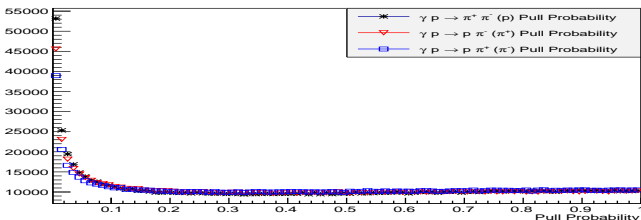


Figure : Kinematic fit pull distribution for the topologies used in the normalization study for data and Monte-Carlo simulation

Table : Binning Used in Efficiency Study

z bins [cm] (5 cm increments)	Momentum bins [GeV]
$-70 \text{ cm} < z < -110 \text{ cm}$	<ul style="list-style-type: none"><li>0 - 0.5</li><li>0.5 - 0.75</li><li>0.75 - 1</li><li>1 - 1.5</li><li>1.5 - 2</li><li>2 - 2.5</li><li>2.5 - 3</li><li>3 - 5</li></ul>

# Normalization of Proton

Proton Data Efficiency at  $-90. < z < -85.$  cm at  $0.75 < P < 1$  GeV

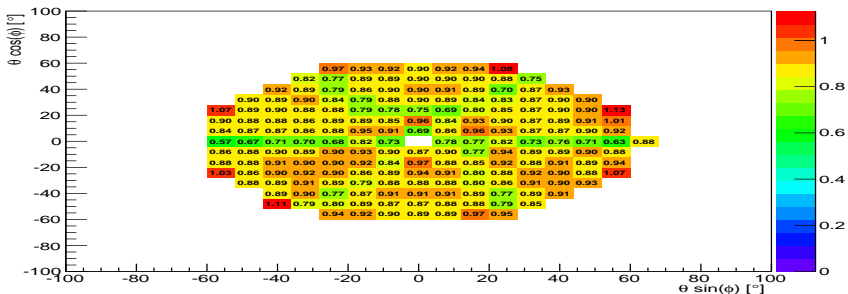


Figure : Plot showing the efficiency of detecting the proton with  $z$ -vertex  $-90 < z < -85$  cm and momentum  $0.75 < P < 1$  GeV from a 2 charged track topology using CLAS detection for g12

# Normalization of Proton

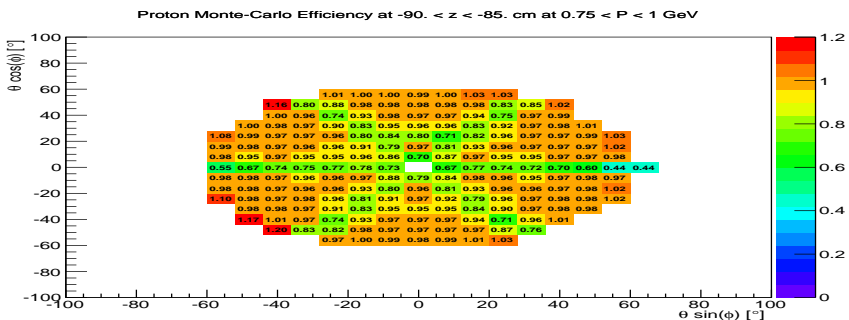


Figure : Plot showing the efficiency of reconstructing the proton with  $z$ -vertex  $-90 < z < -85$  cm and momentum  $0.75 < P < 1$  GeV from a 2 charged track topology using CLAS Monte-Carlo for g12

# Normalization of Proton

Proton Over-Efficiency at  $-90 < z < -85$  cm at  $0.75 < P < 1$  GeV

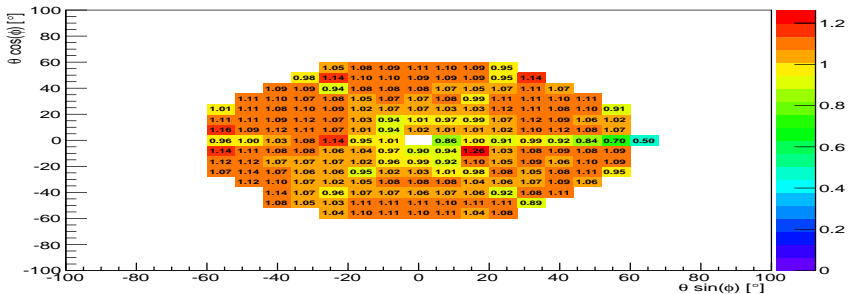


Figure : Plot showing the over-efficiency of simulating the proton with  $z$ -vertex  $-90 < z < -85$  cm and momentum  $0.75 < P < 1$  GeV from a 2 charged track topology using CLAS Monte-Carlo for g12

## Normalization of $pi^+$ and $\pi^-$

- The same procedure was performed for  $pi^+$  and  $\pi^-$  events
- Applied combined normalization for each event
  - $\epsilon = \epsilon_{proton} \cdot \epsilon_{\pi^+} \cdot \epsilon_{\pi^-}$
- Compared results to using static 18% normalization

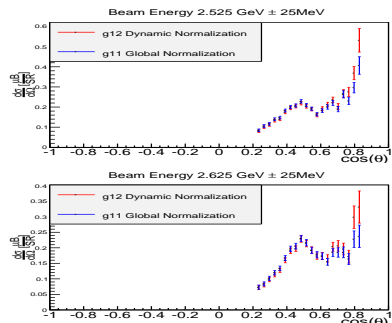
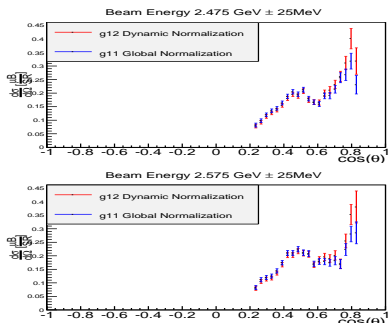


Figure :  $g12 \pi^0$  differential cross-section when the  $g11$  global normalization is used (blue) and when the  $g12$  dynamic normalization is used (red).

# Normalization of $\pi^+$ and $\pi^-$

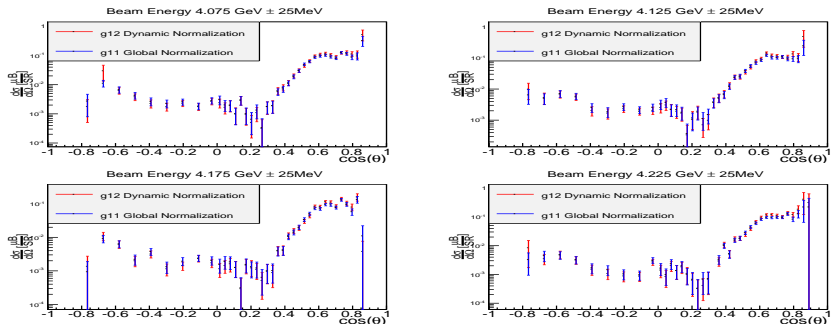


Figure :  $g12\pi^0$  differential cross-section when the  $g11$  global normalization is used (blue) and when the  $g12$  dynamic normalization is used (red).

- The photoproduction amplitude is assumed to a form of a Breit-Wigner and a background term

- $A = A_l(1 + iT_\pi) = A_r \left(\frac{k_0 q_0}{kq}\right)^{\frac{1}{2}} \frac{W_0 \sqrt{\Gamma \Gamma_\gamma}}{W_0^2 - W^2 - iW_0 \Gamma}$
- $A_l$  is the background parameter
- $W_0$ ,  $\Gamma$  and  $\Gamma_\gamma$  are functions of the full width  $\Gamma_0$
- $A_R$  being the resonant parameter

$$A_r = \frac{\mu}{q} \left(\frac{k}{q}\right)^l \sum_{n=0}^N p_n \left(\frac{E_\pi}{\mu}\right)^n$$

- $k_0$  and  $q_0$  are the pion and photon momenta at the resonance energy
- $\mu$  is the pion mass,  $E_\pi$  is the pion kinetic energy in the lab frame and  $p_n$  is a free parameter
- Background term is expanded as a set of Legendre polynomial terms with associated free parameters along with a sum of a pseudoscalar Born partial waves
- Determined by fitting the data. Multi-poles can then be extracted by a fit of  $A$  close to the resonance position.